ORACLE 2-D (v2.0): An efficient module to compute the volatility and oxygen content of organic aerosol with a global chemistry – climate model

Alexandra P. Tsimpidi[1], Vlassis A. Karydis[1], Andrea Pozzer[1], Spyros N. Pandis[2, 3] and Jos Lelieveld[1, 4]

[1] Max Planck Institute for Chemistry, Mainz, Germany

[2] Department of Chemical Engineering, University of Patras, Patras, Greece

[3] Department of Chemical Engineering, Carnegie Mellon University, Pittsburgh, PA, USA

[4] Energy, Environment and Water Research Center, Cyprus Institute, Nicosia, Cyprus

*Corresponding author e-mail: a.tsimpidi@mpic.de

Abstract

A new module, ORACLE 2-D, simulating the organic aerosol formation and evolution in the atmosphere has been developed and evaluated. The module calculates the concentrations of surrogate organic species in two-dimensional space defined by volatility and oxygen-to-carbon ratio. It is implemented into the EMAC global chemistry – climate model, and a comprehensive evaluation of its performance is conducted using an Aerosol Mass Spectrometer (AMS) factor analysis dataset derived from almost all major field campaigns that took place globally during the period 2001-2010. ORACLE 2-D uses a simple photochemical aging scheme that simulates efficiently the net effects of fragmentation and functionalization of the organic compounds. The module predicts not only the mass concentration of organic aerosol (OA) components, but also their oxidation state (in terms of O:C), which allows their classification into primary OA (POA, chemically unprocessed), fresh secondary OA (SOA, low oxygen content) and aged SOA (highly oxygenated). The explicit simulation of chemical OA conversion from freshly emitted compounds to a highly oxygenated state during photochemical aging enables the tracking of hygroscopicity changes of OA that result from these reactions. ORACLE 2-D can thus compute the ability of OA particles to act as cloud condensation nuclei, and serves a tool to quantify the climatic impact of OA.

1. Introduction

Atmospheric aerosols adversely affect human health and play a significant role in climate change on regional and global scales. Depending on their composition, aerosols affect the energy budget of the Earth's atmosphere by scattering and absorbing solar radiation (direct effect) and by influencing the reflective properties of clouds, their lifetime, and precipitation formation (indirect effects). In addition, climate change can play vital and complex role in the formation and removal of atmospheric particles (Trail et al., 2013;Trail et al., 2014). Organic aerosol (OA) is an important constituent of atmospheric particles contributing 20-90% to the total submicron particulate mass, depending on the region (Zhang et al., 2007).

Primary OA (POA) has been traditionally treated as non-volatile and inert in global scale chemistry climate models (CCMs). Robinson et al. (2007) demonstrated that OA emissions are semi-volatile and most of the emitted OA moves to the gas phase after emission due to dilution and evaporation. On the other hand, all organic vapors are subject to photochemical reactions

43 with OH in the gas phase forming organic products with lower volatility that can recondense to
44 the particulate phase as secondary organic aerosol (SOA). To describe the OA gas-aerosol
45 partitioning, Donahue et al. (2006) developed the volatility basis-set (VBS) framework, where
46 OA is assumed to be semi-volatile and photochemically reactive, and is distributed in
47 logarithmically spaced volatility bins. With this innovative approach, the semi-volatile primary
48 emissions, the chemical aging, and the SOA formation were unified within a common framework
49 that is ideally suited for regional and global chemical modeling. Since 2006, many regional
50 (Lane et al., 2008;Murphy and Pandis, 2009;Tsimpidi et al., 2010;Tsimpidi et al., 2011;Ahmadov
51 et al., 2012;Athanasopoulou et al., 2013;Koo et al., 2014;Fountoukis et al., 2014;Ciarelli et al.,
52 2017;Gao et al., 2017) and global (Pye and Seinfeld, 2010;Jathar et al., 2011;Jo et al.,
53 2013;Tsimpidi et al., 2014;Hodzic et al., 2016) modeling studies have used the VBS to account
54 for the semi-volatile nature and chemical aging of organic compounds, demonstrating
55 improvements in reproducing the OA budget and its chemical resolution.

56 The chemical aging of OA results in significant changes of its physical and chemical
57 properties due to the addition of oxygen atoms from the reaction with OH. This increase in OA
58 oxygen content is important for its impact on climate through changes in cloud condensation
59 nuclei (CCN) and ice nuclei (IN) activity. In fact, the oxygen content, expressed by the ratio of
60 oxygen to carbon atoms (O:C), influences the OA hygroscopic growth (Chang et al.,
61 2010;Lambe et al., 2011) which affects CCN activity. In addition, the phase-state changes of
62 SOA during its atmospheric lifetime, which can impact the IN activity, is also influenced by the
63 O:C of the OA (Shiraiwa et al., 2017). Donahue et al. (2011) extended the original one-
64 dimensional VBS framework to two dimensions (2-D VBS) tracking not only the saturation
65 concentration but also the oxygen content of OA during atmospheric transport. This approach
66 further improved the description of the atmospheric evolution of OA and its precursor gases that
67 become increasingly more oxidized, less volatile, and more hygroscopic during their atmospheric
68 aging. However, the large number of additional surrogate organic compounds required by the 2-
69 D VBS framework has hindered implementation in three-dimensional atmospheric models
70 (Napier et al., 2014). Therefore, the 2-D VBS approach has been mostly adopted in box and 1-D
71 Lagrangian models (Murphy et al., 2011;Murphy et al., 2012;Chacon-Madrid et al., 2013;Zhao et
72 al., 2015;Paciga et al., 2016). Koo et al. (2014) introduced a hybrid VBS approach for use in
73 three dimensional chemical transport models (CTMs) which combines the simplicity of the VBS

74 with the ability to track the evolution of OA in the 2-D space of volatility and oxygen content.

75   In this work, the computationally efficient module for the description of OA composition and

76 evolution in the atmosphere (ORACLE; Tsimpidi et al., 2014) has been extended to allow for the

77 first time in a global CCM the description of both the volatility and the oxygen content of OA

78 based on the 2-D VBS approach. Similar to ORACLE v1.0, the interface of the new version

79 allows the user to have full control of the complexity of the OA scheme by adjusting the number

80 of species and reactions (i.e., number of compounds, volatility bins, O:C bins) to optimize the

81 computational cost according to the application and the desired chemical resolution. The updated

82 ORACLE module can provide valuable information about the physicochemical evolution of OA

83 during its atmospheric lifetime in support of modeling studies and help quantify the climatic

84 impact of OA.

85

86 **2. Model description**

87 **2.1 EMAC model**

88   The ECHAM/MESSy Atmospheric Chemistry (EMAC) model is a numerical chemistry

89 and climate simulation system that includes sub-models describing lower and middle

90 atmospheric processes and their interaction with oceans, land, and human influences. EMAC

91 consists of the Modular Earth Submodel System and an advanced version of the 5th generation

92 of the European Centre Hamburg (ECHAM) general circulation model. ECHAM5 (Roeckner et

93 al., 2006) serves as the atmospheric dynamic core that simulates the atmospheric flow and is

94 integrated in the base model layer of MESSy. The interface structure of MESSy links the base

95 model with several atmospheric submodels that simulate online the gas-phase chemistry

96 (MECCA; Sander et al., 2011), inorganic aerosol microphysics and dynamics (GMXe; Pringle et

97 al., 2010), organic aerosol formation and growth (ORACLE; Tsimpidi et al., 2014), emissions

98 (ONLEM and OFFLEM; Kerkweg et al., 2006b), dry deposition and sedimentation (DRYDEP

99 and SEDI; Kerkweg et al., 2006a), cloud scavenging (SCAV; Tost et al., 2006), cloud

100 microphysics (CLOUD; Jöckel et al., 2006;Bacer et al., 2018), and aerosol optical properties

101 (AEROPT; Lauer et al., 2007). EMAC has been extensively described and evaluated against

102 ground-based and satellite observations (Pozzer et al., 2012;Tsimpidi et al., 2014;Tsimpidi et al.,

103 2016, 2017;Karydis et al., 2016;Karydis et al., 2017). In this study, the applied spectral

104 resolution of the EMAC model is T63L31, corresponding to a horizontal grid resolution of

105   1.875ºx1.875º and 31 vertical layers extending to 18 km altitude (10hPa). EMAC is applied for

106   11 years covering the period 2000-2010 and the first year is used as spin-up.

107

2.2 ORACLE module

2.2.1 Module description

110   ORACLE is a computationally efficient module for the description of organic aerosol

111   composition and evolution in the atmosphere (Tsimpidi et al., 2014) that has been incorporated

112   into the EMAC model. The original version of ORACLE (V1.0) simulated the volatility

113   distribution of a wide variety of semi-volatile organic surrogate compounds using bins of

114   logarithmically spaced effective saturation concentrations. Organic emissions from multiple

115   anthropogenic and natural sources are taken into account using distinct surrogate species for each

116   source category. These surrogates can be subdivided into groups of organic compounds based on

117   their volatility: Low volatility organic compounds (LVOCs, $C* \leq 10^{-1}$ µg m^{-3}), semi-volatile

118   organic compounds, (SVOCs, $10^{-1} < C* \leq 10^2$ µg m^{-3}), intermediate volatility organic compounds

119   (IVOCs, $10^2 < C* \leq 10^6$ µg m^{-3}) and volatile organic compounds (VOCs, $C* > 10^6$ µg m^{-3}). These

120   organic compounds are allowed to partition between the gas and aerosol phases resulting in the

121   formation of OA. The change in aerosol mass of each size mode after the phase partitioning is

122   determined by using a weighting factor as described in Tsimpidi et al. (2014). Gas-phase

123   photochemical reactions that modify the volatility of the organics are taken into account and the

124   oxidation products of each group of precursors are simulated separately in the module to keep

125   track of their origin. The model results for the different organic components in the particulate

126   phase were compared with factor analysis results derived from a comprehensive dataset of aerosol

127   mass spectrometer (AMS) measurements from multiple field campaigns across the Northern

128   Hemisphere. The resulting good agreement between campaign average concentrations and model

129   predictions supports the capability of the model to capture the spatial and temporal characteristics

130   of OA levels. Tsimpidi et al. (2017) conducted an extensive sensitivity analysis of the EMAC OA

131   predictions to uncertain parameters in the ORACLE module. One of the major conclusions of

132   their analysis was that the model performance can be improved by assuming that freshly emitted

133   organic compounds are relatively hydrophobic and become increasingly hygroscopic due to

134   oxidation. As a first step to achieve this goal, the ORACLE module has been further developed

here to account for the oxidation state of the organic surrogate compounds. The new version is called ORACLE 2-D.

2.2.2. Emission inventory of OA precursors

The emissions of biogenic VOCs (i.e., isoprene and monoterpenes) are calculated online by EMAC with the ONLEM submodel. The open biomass burning emissions of organic compounds from savanna and forest fires are based on the Global Fire Emissions Database (GFED version 3.1; van der Werf et al., 2010) and are distributed into LVOCs (20%), SVOCs (40%), and IVOCs (40%) based on the emission factors proposed by May et al. (2013). The emissions of anthropogenic LVOCs, SVOCs, IVOCs, and VOCs (i.e., aromatics, alkanes, olefins) from fossil and biofuel combustion are derived from the CMIP5 emission inventory for the RCP4.5 scenario (Thomson et al., 2011). The volatility distribution of anthropogenic emissions to LVOCs (8%), SVOCs (72%), and IVOCs (170%) is based on the findings of (Robinson et al., 2007) and includes increased factors (the sum of the emission factors is 250%) to account for the missing IVOC emissions from the traditional inventories. More details about the organic compound emissions used here can be found in Tsimpidi et al. (2016).

3 ORACLE 2-D description

3.1 Module overview

The original ORACLE v1.0 (called hereafter ORACLE) uses saturation concentration bins to describe the volatility distribution of the major OA components. In this work, ORACLE is extended to also resolve the oxygen content of OA expressed by the O:C ratio (ORACLE v2.0; called hereafter ORACLE 2-D). The volatility dimension is discretized in up to 10 logarithmically-spaced volatility bins separating the organic compounds in low volatility (LVOCs, expressed by the volatility bins of 10^{-3}, 10^{-2}, and 10^{-1} µg m^{-3}), semi-volatile (SVOCs, C^* equal to 10^0, 10^1, and 10^2 µg m^{-3}), and those of intermediate volatility (IVOCs, C^* equal to 10^3, 10^4, 10^5 and 10^6 µg m^{-3}). Extremely low volatility organic compounds (ELVOCs, $C^* \leq 10^{-4}$) can be formed by the ozonolysis of monoterpenes and sesquiterpenes (Liggio et al., 2010;Sun et al., 2009) playing an important role for the formation and growth of new particles created in situ in the atmosphere by nucleation (Ehn et al., 2014). The production of ELVOCs from biogenic VOCs is not currently included in ORACLE since the simulation of new particle formation is

166   outside the scope of the current article, and part of work in progress. In addition, the oxygen

167   content dimension is discretized in up to 20 linearly spaced O:C bins subdividing the organic

168   compounds into fresh emissions (expressed by the O:C bins of 0.1 and 0.2), less oxygenated

169   organic compounds (O:C equal to 0.3, 0.4, 0.5, and 0.6), moderately oxygenated organic

170   compounds (O:C equal to 0.7, 0.8, 0.9, and 1.0), and highly oxygenated species with O:C>1. The

171   first bin includes also the hydrocarbons with zero oxygen. The O:C range can be extended up to

172   2 (for CO_2). However, there are only a few atmospheric organic compounds with O:C higher

173   than unity and the observed O:C of ambient OA rarely exceeds 1.1 (Ng et al., 2010; Kroll et al.,

174   2011). The ability of ORACLE 2-D to simulate degree of oxidation of OA allows the simulation

175   of its hygroscopicity by using proposed parameterizations that link the hygroscopicity parameter

176   kappa with the O:C of OA (Chang et al., 2010;Lambe et al., 2011;Kuwata and Lee, 2017). In the

177   current application, the hygroscopicity of each OA compound is represented by a linear function

178   of the form κ_{org}=0.18 (O:C) + 0.03 (Lambe et al., 2011).

179   ORACLE 2-D has a flexible interface in which the user can choose the resolution

180   (number of bins used in each dimension) of the 2-D VBS space through a namelist file

181   depending on the desired application and scientific goals. The namelist file includes the variables

182   that control the desired chemical resolution of OA (number of volatility/O:C bins, number of size

183   modes, saturation concentrations, molecular weights, etc.) and the desired emission factors for

184   the distribution of POA emissions into LVOC, SVOC and IVOC volatility bins (and the

185   corresponding O:C bins). Changes to the gas-phase chemistry (e.g., photochemical reaction rate

186   constants) need to be made in the MECCA submodel by modifying the ORACLE replacement

187   file, which will automatically update the gas phase chemistry used by EMAC. Then, the interface

188   layer of ORACLE 2-D reads the namelist variables and automatically i) defines the new tracers

189   for organic compounds, ii) performs the coupling with the emission modules and with the gas-

190   phase chemistry module (MECCA), and iii) calls the core layer of the ORACLE 2-D module.

191   The core layer calculates the bulk equilibrium gas and aerosol concentrations and distributes the

192   change in the bulk aerosol concentration into size modes.

193   In this work, we employ ORACLE 2-D based on the sensitivity analysis results of

194   Tsimpidi et al. (2017) and using the 2-D VBS at a resolution suitable for medium-term

195   simulations with global chemistry-climate models. This chemical resolution includes 150 organic

196 aerosol surrogate compounds, compared to 34 OA compounds in ORACLE, which result in a
197 16% increase of the overall EMAC computational burden. The performance reduction comes
198 mainly from the gas phase chemistry and secondarily from the atmospheric transport of the
199 additional tracers, since ORACLE 2-D uses an efficient method to minimize the computational
200 cost of the phase partitioning calculations as described in section 3.4.

201

202 **3.2 Constructing the two dimensional grid**

203 For the current application, ORACLE 2-D distributes the OA surrogate species into
204 logarithmically spaced volatility bins with C^* varying from 10^{-2} to 10^6 µg m^{-3} and linearly spaced
205 oxygen content bins with O:C varying from 0.1 to 1.2 (Figure 1). Each of the OA surrogate
206 species in this C^*-O:C 2-D space is characterized by a representative number of carbon atoms per
207 molecule (n_C) and a molecular weight (MW). Donahue et al. (2011) used structure activity
208 relationships (Pankow and Asher, 2008) to express the C^* as a function of n_c and the number of
209 oxygens per molecule (n_o):

210
$$\log_{10} C^* = 0.475(25 - n_C) - 2.3n_O + 0.6\frac{n_C n_O}{n_C + n_O} \quad (1)$$

211

212 Given that n_o is a function of O:C and n_c:

213

214
$$n_O = n_C(\text{O:C}) \quad (2)$$

215

216 n_c can be expressed as a function of C^* and O:C:

217
$$n_C = \frac{11.875 - \log_{10} C^*}{0.475 + 2.3(\text{O:C}) - 0.6\frac{(\text{O:C})}{1 + (\text{O:C})}} \quad (3)$$

218

219 Assuming that the organic compounds consist entirely of carbon, oxygen, and hydrogen atoms
220 (i.e., ignoring nitrogen and sulfur), the MW of each surrogate species is a function of n_C, n_O,
221 and the number of hydrogen atoms per molecule (n_H) and therefore it can be calculated as:

222

$$MW = n_H + 16n_O + 12n_C \qquad (4)$$

224   where,

225

$$n_H = n_C(\text{H:C}) \qquad (5)$$

227

228   H:C is the atomic ratio of hydrogen to carbon approximated by Heald et al. (2010) as:

229

$$\text{H:C} = 2 - (\text{O:C}) \qquad (6)$$

231

232   Combining Equations 4, 2, and 5, we get

233

$$MW = (15(\text{O:C}) + 14)n_C \qquad (7)$$

235

236   Given that n_c decreases as C^* increases (Eq. 3), the MW calculated by Eq. 7 is consistent with the
237   molecular corridor approach (Shiraiwa et al., 2014) which suggests a tight inverse correlation
238   between volatility and molar mass constrained by boundary lines of low and high O:C ratios.

239   Organic compound emissions from anthropogenic fuel combustion and open biomass
240   burning include LVOCs (with C^* at 298 K equal to 10^{-2} µg m^{-3}) SVOCs (with C^* at 298 K equal
241   to 10^0 and 10^2 µg m^{-3}) and IVOCs (with C^* at 298 K equal to 10^4 and 10^6 µg m^{-3}). Their
242   corresponding emissions are estimated using the emission factors of Tsimpidi et al. (2016).
243   Freshly emitted LVOCs, SVOCs, and IVOCs from anthropogenic and open biomass burning
244   sources are assigned an initial O:C of 0.1 (Figure 1a) and 0.2 (Figure 1b), respectively (Donahue
245   et al., 2011). We distinguish anthropogenic and biogenic VOCs, and their first generation
246   oxidation products are distributed in four volatility bins (with C^* at 298 K equal to 10^0, 10^1, 10^2,
247   and 10^3 µg m^{-3}) by using the aerosol mass yields by Tsimpidi et al. (2014). The O:C distributions
248   of the first generation VOC oxidation products are given by Murphy et al. (2011) and vary with
249   volatility (Figures 1c and 1d).

250

3.3 New photochemical aging scheme

Similar to ORACLE, multiple generations of homogeneous gas-phase reactions with OH are simulated for all OA compounds treated by ORACLE 2-D. After each oxidation step, oxygen atoms are added to the reacting organic gas resulting in an increase of oxygen content and a change of volatility due to functionalization (reducing the volatility) or fragmentation (increasing the volatility). To minimize the computational cost and at the same time simulate the net effect of both fragmentation and functionalization, ORACLE 2-D uses an approach similar to the aging scheme proposed by Murphy et al. (2011). ORACLE 2-D assumes a net average decrease in volatility of aSOA-v (SOA from the oxidation of anthropogenic VOCs) reacting with OH by a factor of 10 and the addition of one or two oxygen atoms with the same probability of 50% (Figure 1c). Assuming volatility transformations only into one direction (functionalization) and neglecting fragmentation can lead to increasingly higher OA concentrations in lower volatility bins. This may result in an overestimation of OA at long aging time scales up to thousands of kilometers downwind of the source regions. However, this overestimation can be partially offset by the conservative aging scheme used in ORACLE 2-D, compared to the relatively aggressive functionalization scheme proposed by (Murphy et al., 2012). The same addition of oxygen atoms (one or two) is assumed for bSOA-v (SOA from the oxidation of biogenic VOCs), however, its volatility remains unchanged due to a balancing of fragmentation and functionalization effects (Murphy et al., 2012) (Figure 1d). The OH reaction rate constant for both aSOA-v and bSOA-v is 1×10^{-11} cm^3 molecule^{-1} s^{-1} (Donahue et al., 2006;Tsimpidi et al., 2010). The reaction of SOA-sv (SOA from the oxidation of SVOCs) and SOA-iv (SOA from the oxidation of IVOCs) with OH with a rate constant of 2×10^{-11} cm^3 molecule^{-1} s^{-1} (Tsimpidi et al., 2014) results in the addition of two or three oxygen atoms (with equal probability) and the reduction of their volatilities by a factor of 100 (Figure 1a, 1b). The number of added oxygen atoms (n_{O+}) due to the reaction with OH is then expressed as an increase of O:C in the 2-D space. Each of the OA surrogate compounds in the 2-D space described in Section 3.3 has a representative number of carbon per molecule (n_C). Assuming that carbon is conserved during the reaction with OH, the O:C of the product is calculated as follows:

280
$$(O:C)_{product} = (O:C)_{reactant} + \frac{n_{O+}}{n_C} \quad (8)$$

281

282 If the $(O:C)_{product}$ has more than one decimal places, then is distributed between the two adjacent

283 O:C bins of the 2-D space by using linear interpolation. Finally, since carbon is conserved, the

284 increase in organic mass (OM) due to the added oxygen after each oxidation reaction is

285 calculated as:

286

287
$$\frac{OM_{product}}{OM_{reactant}} = \frac{\left(\dfrac{OM}{OC}\right)_{product}}{\left(\dfrac{OM}{OC}\right)_{reactant}} \quad (9)$$

288

289 where, following Murphy et al. (2011),

290

291
$$\left(\frac{OM}{OC}\right) = 1 + \frac{16}{12}(O:C) + \frac{1}{12}(H:C) \quad (10)$$

292

293 **3.4 Phase partitioning calculations**

294   ORACLE 2-D uses the core layer of the ORACLE module to calculate the partitioning of

295 organic compounds between the gas and particle phases by assuming bulk equilibrium (Tsimpidi

296 et al., 2014). However, the computational time required for the phase partitioning increases

297 super-linearly with the number of species. As the condensation/evaporation of organic

298 compounds depends only on their saturation concentration and not their O:C ratio, only one

299 equilibrium calculation is performed per volatility bin of each category (i.e., fuel combustion,

300 biomass burning, anthropogenic VOC products, and biogenic VOC products). This approach

301 reduces significantly the number of equations to be solved and the corresponding computational

302 cost of the phase partitioning calculations.

303   The ORACLE core layer calculates the aerosol composition at equilibrium by solving the

304 following set of *n* nonlinear equations:

305

$$C_{a,i} = C_{t,i} - x_i C_i^* \text{ for } i = 1, n \quad (11)$$

307

$$x_i = \frac{C_{a,i}/M_i}{\sum_{i=1}^{n} C_{a,i}/M_i} \quad (12)$$

309

where $C_{t,i}$ and $C_{a,i}$ are the total and aerosol-phase concentrations of product i in µg m^{-3}, respectively, C_i^* is the effective saturation concentration of species i, x_i is the mole fraction of product i in the absorbing organic phase, and M_i is the molecular weight of product i which corresponds to the weighted average molecular weight of the species with the same saturation concentration.

The temperature dependence of the saturation concentrations is described by the Clausius–Clapeyron equation:

$$c_i^* = c_{i,0}^* \frac{T_0}{T} \exp\left[\frac{\Delta H}{R} \left(\frac{1}{T_0} - \frac{1}{T} \right) \right] \quad (13)$$

where c_i^* and $c_{i,0}^*$ are the saturation concentrations at temperature T and T_0, respectively, R is the gas constant, and ΔH is the enthalpy of vaporization. Here, an effective $\mathit{\Delta H}$ of 30 kJ mol^{-1} is used for all aSOA-v and bSOA-v species based on data for α-pinene (Pathak et al., 2007). A $\mathit{\Delta H}$ of 112 , 100, 88, 76, and 64 kJ mol^{-1} is used for the 10^{-2}, 10^0, 10^2, 10^4, and 10^6 µg m^{-3} volatility bins, respectively, of all organic compounds from fuel combustion and biomass burning sources based on data for large saturated species commonly found in primary emissions (Donahue et al., 2006).

Water uptake by the particulate organic phase under high relative humidity conditions can increase the aerosol mass and decrease the mole fraction of individual organic products which may allow additional condensation of SOA (Jathar et al., 2016). However, Eq. 12 calculates the mole fraction of organic products only in the absorbing organic phase without taking into account the presence of water in aerosol phase. This simplification can result in an underestimation of SOA in areas with high humidity and significant SOA concentrations.

331   Assuming that the distribution of the species of the same volatility bin in the different O:C

332   bins does not change due to the condensation or evaporation, the gas and aerosol concentrations

333   of each compound in the 2-D space after the phase partitioning calculations are given by:

334

335
$$SOG_{i,j}(t+\Delta t) = \left(\sum_{j=1}^{m} SOG_{i,j}(t+\Delta t) \right) \frac{SOG_{i,j}(t) + SOA_{i,j}(t)}{\sum_{j=1}^{m} SOG_{i,j}(t) + \sum_{j=1}^{m} SOA_{i,j}(t)} \quad (13)$$

336

337   and

338

339
$$SOA_{i,j}(t+\Delta t) = \left(\sum_{j=1}^{m} SOA_{i,j}(t+\Delta t) \right) \frac{SOG_{i,j}(t) + SOA_{i,j}(t)}{\sum_{j=1}^{m} SOG_{i,j}(t) + \sum_{j=1}^{m} SOA_{i,j}(t)} \quad (14)$$

340

341   where, SOG and SOA are the gas and aerosol concentrations of each compound, respectively, i

342   and j are the volatility and O:C bin index in the 2-D space, respectively, m is the total number of

343   O:C bins, and t and $t+\Delta t$ are the times before and after the phase partitioning calculations,

344   respectively. $\sum_{j=1}^{m} SOG_{i,j}(t+\Delta t)$ and $\sum_{j=1}^{m} SOA_{i,j}(t+\Delta t)$ for each volatility bin i in eqs. 13 and 14

345   correspond to $C_{a,i}$ and $(C_{t,i} - C_{a,i})$ at equilibrium calculated from eqs. 11 and 12.

346

347

348   **4. Model results**

349   **4.1 Total OA and O:C**

350   Simulated total OA concentrations are high over regions affected by anthropogenic fuel

351   combustion and open biomass burning (Figure 2a). The highest annual average OA

352   concentrations at the surface are predicted over the densely populated areas of Eastern China,

353   Northern India and Bangladesh (10-28 μg m^{-3}), as well as over the tropical forest in the Congo

354   Basin (12-22 μg m^{-3}). Considerably high OA concentrations are also predicted over the tropical

355   forests of Southeast Asia and the Amazon (6-17 μg m^{-3}). Strong fossil fuel combustion sources

356   over the Arabian Peninsula result in annual average OA concentrations of 6-10 μg m^{-3}. The

357 calculated zonal average concentrations of total OA at surface peak over the mid-latitudes of the

358 Northern Hemisphere and the tropics (~ 4 µg m^{-3}) remain relatively high (>2 µg m^{-3}) up to 750

359 hPa altitude (Figure 2b). Over Europe, predicted OA annual average concentrations at the ground

360 level are in the 3-7 µg m^{-3} range. Over North America, the highest OA concentration is simulated

361 over Southern California, and also over the Mexico City metropolitan area, and the Southeastern

362 USA (2-8 µg m^{-3}). OA concentrations in the 0.5-1 µg m^{-3} range are predicted over parts of the

363 oceans due to the long-range transport of OA from the adjacent continental sources. Non-

364 negligible concentrations of OA can be found over the Greenland and Antarctica due to the long-

365 range transport of organic compounds and their condensation in the particulate phase under very

366 low temperatures. The calculated total tropospheric OA burden is 3.3 Tg, which is higher

367 compared to the calculated tropospheric burden of ORACLE v1.0 (2 Tg; Tsimpidi et al., 2016)

368 but is within the range of OA tropospheric burdens (0.7 to 3.8 Tg) from 31 global CTMs

369 reported by Tsigaridis et al. (2014).

370 Figure 3a depicts the annual average simulated O:C ratio of total OA at the surface.

371 Lower values of O:C are predicted close to OA sources, i.e., over the industrialized areas of the

372 Northern Hemisphere, and over the tropical and boreal forests. The lowest average values occur

373 over the boreal forests (as low as 0.3) due to the limited photochemical activity over these

374 regions, in contrast to the tropical forests, where O:C is around 0.5. Over the densely populated

375 areas of Asia, Europe and North America, the O:C is about 0.3-0.4, i.e., close to the

376 anthropogenic sources. O:C levels increase rapidly (in excess of 0.6) downwind of the sources

377 due to photochemical aging of the transported OA. The highest O:C values are calculated over

378 the Sahara Desert and the remote Atlantic and Pacific Oceans (0.8-1), however, over these

379 regions, OA concentrations are low (Figure 2). O:C ratios increase significantly with altitude

380 according to the model (Figure 3b) since organic vapors transported vertically react with OH,

381 forming products with higher oxygen content. Over the mid-latitudes of the Northern

382 Hemisphere, the average O:C ratio near the surface is 0.55, and increases as the air masses are

383 transported aloft by approximately 0.05 for every 100 hPa (Figure 3b).

384

385 **4.2 POA and SOA**

386 Figure 4a depicts the decadal average simulated POA concentrations at the surface. POA

387 concentrations are high over the densely populated areas of the Northern Hemisphere due to

388 strong fuel combustion emissions from the industrial, energy, residential and transport sectors.

389 The highest concentrations are calculated over Eastern China (3-13 μg m^{-3}), Bangladesh (2-8 μg

390 m^{-3}), and Eastern Europe (1-3 μg m^{-3}). Open biomass burning emissions from forest, woodland,

391 peatland and savannah fires result in high POA concentrations over the tropics (3-8 μg m^{-3} over

392 the Congo Basin) and the boreal forests (1-6 μg m^{-3} over Russia). However, a large fraction of

393 POA evaporates due to dilution as the air masses travel downwind from the sources, resulting in

394 significant reduction of the concentration (Figure 4a). Then, the material that is transferred to the

395 gas phase can be oxidized and recondense to the aerosol phase forming SOA that persists even

396 far from the sources (Figure 4b). This results in a relatively homogeneous regional distribution

397 of SOA with a continental background of 2 μg m^{-3} and high concentrations even far downwind

398 from anthropogenic (e.g., 7-22 μg m^{-3} over South and Eastern Asia) and open biomass burning

399 (e.g., 9-17 μg m^{-3} over Central Africa) sources. Lower concentrations are predicted over the

400 boreal forests (~1 μg m^{-3}) due to minor photochemical activity.

401   The tropospheric burden of POA and SOA calculated by ORACLE 2-D is 0.25 Tg and

402 3.05 Tg, respectively. While the value of POA is very similar to the corresponding tropospheric

403 burden of ORACLE (0.24 Tg), the tropospheric burden of SOA has increased significantly (1.74

404 Tg in ORACLE). The tropospheric burden of POA calculated by ORACLE 2-D is much lower

405 than most global CTMs in the AEROCOM intercomparison study (mean value of 0.85 Tg)

406 (Tsigaridis et al., 2014). This difference is due to the evaporation of POA and its conversion into

407 SOA in ORACLE 2-D, given that this dynamic behavior of POA is not taken into account by

408 most global CTMs. Consequently, the ORACLE 2-D calculated SOA tropospheric burden is

409 higher than most CTMs from the AEROCOM intercomparison study (mean value of 1 Tg)

410 (Tsigaridis et al., 2014) due to its stronger chemical production. As indicated by Tsimpidi et al.

411 (2016), the POA burden is underestimated by our model, especially in the urban environment in

412 the winter. This underestimation was partially attributed to missing residential wood burning

413 emissions in our inventory (van der Gon et al., 2015).

414

415 **4.3 Fresh and aged SOA**

416   The major advantage, at least in this initial phase, of extending the ORACLE module to

417 describe the oxygen content of OA is the model's ability to quantify the degree of photochemical

418 processing of the OA. The model can distinguish the fresh SOA that is relatively less oxygenated

419 and the highly aged and oxygenated SOA. As a first approximation, OA compounds with O:C ≤

420 0.6 are considered "fresh SOA" and OA compounds with O:C > 0.6 are considered as "aged

421 SOA".

422   Figure 5 depicts the average concentrations of fresh and aged SOA and their fractional

423 contributions to total SOA at the surface. Fresh SOA exceeds aged SOA close to the source areas

424 (Figures 5c). On the other hand, the spatial distribution of aged SOA extends further from the

425 sources with relatively high concentrations even over remote continental (e.g., Sahara) and

426 oceanic (e.g., North Pacific) regions (Figure 5b). Aged SOA maximizes over north India since

427 southerly monsoon winds, prevailing during summer, favor the transport of aged organic

428 compounds to the north where they can accumulate at the foothills of the Himalaya mountain

429 range before being removed by convection and precipitation. The fraction of aged SOA is higher

430 over the industrialized regions (0.4-0.7), where IVOCs comprise 70% of total fuel combustion

431 emissions, and lower over the tropics (0.1-0.5), where IVOCs represent 40% of total open

432 biomass burning emissions (Figure 5d). Overall, the tropospheric burden of fresh SOA is 1.26 Tg

433 and of aged SOA 1.79 Tg.

434   The simulated vertical profiles of fresh and aged SOA are quite different (Figure 6). Both

435 fresh and aged SOA concentrations are high near the surface with zonal averages of 0.9-1.7 μg

436 m^{-3} over the northern mid-latitudes and the tropics. However, at higher altitudes the oxidation of

437 fresh SOA continues, which leads to the transformation into aged SOA. Therefore, above 960

438 hPa altitude the zonal average concentrations of fresh SOA decrease gradually (below 1 μg m^{-3})

439 and that of aged SOA increase, exceeding in some cases 1.5 μg m^{-3} at 850 hPa altitude. Further

440 aloft in the atmosphere (above 700 hPa altitude) the levels of both fresh and aged SOA are

441 reduced significantly due to dilution and removal.

442

443 **4.3 2-D space distribution**

444   In this section, we present a new feature that comes along with the upgraded ORACLE 2-D.

445 Since ORACLE 2-D explicitly describes the concentration of organic surrogate species in two

446 dimensional space, defined by their volatility and O:C ratio, it can also provide as output its

447 distribution in this 2-D space. As an example, Figure 7 depicts the 2-D distribution of the

448 average total OA concentrations during the years 2001-2010 over central Europe and the

449   Amazon basin. The first left column represents all the species with $C^* \leq 10^{-2}$ μg m^{-3}, while the top
450   line represents all the species with O:C ≥ 1.2.

451   Over Europe, approximately 50% of OA has $C^* = 1$ μg m^{-3}. About 10% of the OA is
452   emitted directly in this volatility bin as POA with O:C = 0.1, while the rest, 40%, is SOA with
453   higher O:C from the aging of more volatile compounds. The volatility bin with $C^* = 10^{-2}$ μg m^{-3}
454   is also important, containing 18% of the total OA. On the other hand, volatility bins with $C^* >$
455   10^2 contain less than 1% of total OA since organic species in these high volatility bins exist
456   mainly in the gas phase. Furthermore, about 30% of the total OA over Europe has O:C≤0.2,
457   mainly from direct emissions of POA from fuel combustion sources with O:C=0.1 (20% of total
458   OA). Organic species with O:C = 0.4 are also important, representing 15% of the total OA.
459   Overall, 40% of OA over Europe has 0.3≤O:C≤ 0.6 and 30% is highly oxidized with O:C≥0.7.

460   Over the Amazon, similar to Europe, approximately 50% of total OA has $C^* = 1$ μg m^{-3}
461   while bins with $C^* > 10^2$ contain only 2% of total OA. However, volatility bins with $10^2 \leq C^*$
462   ≤10^3 are more important compared to Europe containing about 30% of the total OA
463   concentrations. This discrepancy can be attributed to the high bSOA-v concentrations over the
464   Amazon rainforest, which remain within higher volatility bins during their photochemical aging
465   compared to aSOA-v. Furthermore, similar to Europe, about 30% of total OA over the Amazon
466   has O:C ≤ 0.2, mainly affected by the direct aerosol emissions from biomass burning with O:C =
467   0.2 (~20% of total OA). OA species with 0.3≤O:C≤0.6 represent 55% of the total OA with
468   mostly O:C = 0.4 (35% of total OA). On the other hand, only 15% of the total OA is highly
469   oxidized with O:C ≥ 0.7. Comparing these results to Europe shows that OA over biomass
470   burning areas (e.g., the Amazon) are estimated to be less oxidized than OA over anthropogenic
471   areas (e.g., Europe), despite the higher photochemical activity over the tropics. This perhaps
472   unexpected result can be explained by the higher fraction of IVOC emissions over the
473   industrialized regions that can increase the overall oxidation state of OA through their multi-
474   generational aging.

475

476   **5. Model performance evaluation**

477   The mean absolute gross error (MAGE), mean bias (MB), normalized mean error (NME),
478   normalized mean bias (NMB), and the root mean square error (RMSE) are used to assess the

479 model performance of the simulations of OA components (i.e., POA, fresh and aged SOA) and

480 O:C (Tsimpidi et al., 2016).

481

482 **5.1 Organic aerosol concentrations**

483 The simulated POA and SOA can be compared against AMS factor analysis results from

484 61 field campaigns performed during the period 2001–2010 over urban-downwind and rural

485 environments in the Northern Hemisphere (Figure 8). Information for each of these campaigns is

486 given in Tsimpidi et al. (2016). Factor-analysis techniques classify OA into hydrocarbon-like OA

487 (HOA), biomass burning OA (BBOA), and oxygenated OA (OOA). HOA is assumed to

488 correspond to POA from fossil fuel combustion, and BBOA corresponds to POA from biomass

489 burning (Crippa et al., 2014). Therefore, simulated POA is compared here against the sum of

490 AMS HOA and BBOA (Table 1). OOA corresponds to modelled SOA (Table 2) and can be

491 further classified into two subtypes, semi-volatile OOA (SVOOA) and low volatility OOA

492 (LVOOA) (Crippa et al., 2014). Recent studies have suggested that the main difference between

493 these two OOA types is often not so much their volatility, but mostly their oxygen content

494 (Kostenidou et al., 2016; Louvaris et al., 2017). These two OOA types represent distinct

495 oxidation states with O:C of 0.33-0.67 for SVOOA and 0.67-1.00 for LVOOA (Donahue et al.,

496 2012). Therefore, SVOOA can be compared at least as a zero-order approximation against the

497 simulated fresh SOA (Table 3) and LVOOA against the simulated aged SOA (Table 4).

498 The model reproduces the observed campaign average POA concentrations within a factor of

499 two in 40% of the cases over urban downwind and rural locations (Table 1, Figure 8a). The

500 average simulated POA concentration over the urban downwind regions is around 0.65 $\mu g\ m^{-3}$

501 and it decreases further after continued transport from the sources to 0.45 $\mu g\ m^{-3}$ over the rural

502 areas. Compared to AMS HOA concentrations, modelled POA is unbiased over rural

503 environments, however, it is underestimated downwind of urban areas (MB=-0.17 $\mu g\ m^{-3}$). The

504 model has the best performance during summer with MB=-0.05 $\mu g\ m^{-3}$ and RMSE = 0.40 $\mu g\ m^{-3}$

505 ^{3}. Compared to ORACLE (Tsimpidi et al., 2016), ORACLE 2-D produces almost identical

506 concentrations of POA, hence the model performance is unchanged.

507 Calculated SOA concentrations are higher than POA both downwind of major urban centers

508 (2.76 $\mu g\ m^{-3}$) and rural locations (2.53 $\mu g\ m^{-3}$). The model reproduces the observed campaign

509 average SOA concentrations within a factor of two in 65% of the cases over urban downwind

510 and rural locations. Simulated average SOA concentrations are slightly low-biased compared to

511 AMS OOA measurements downwind of urban areas (MB=-0.22 μg m^{-3}) and over rural areas

512 (MB=-0.18 μg m^{-3}). While the model performs well during spring (NMB=11%), summer

513 (NMB=-10%), and autumn (NMB=0%), it strongly underestimates SOA concentrations during

514 winter (NMB=-76%). This underestimation of SOA by the model is mostly due to missing

515 LVOOA. For the 41 campaigns in which both OOA types were identified, EMAC reproduces the

516 fresh SOA concentrations well (compared to SVOOA) with a MB of 0.41 and 0.32 μg m^{-3}

517 downwind of urban and in rural locations, respectively (Table 4). Furthermore, except during

518 winter, the model is also able to capture the seasonal variations of the fresh SOA concentration

519 (Table 4). However, the model underpredicts the aged SOA concentrations (compared to AMS

520 measured LVOOA) with a MB of -0.95 and -0.70 μg m^{-3} over urban downwind and rural

521 locations, respectively. This aged SOA underestimation is also evident during the four seasons of

522 the year and especially during winter (NMB = -93%). This result may indicate that the model

523 underestimates the atmospheric aging rate of SOA or misses processes forming highly oxidized

524 OA, e.g., highly oxidized ELVOCs from the ozonolysis of terpenes (Ehn et al., 2014; Jokinen et

525 al., 2016). Therefore, another useful feature of ORACLE 2-D is that detailed AMS

526 measurements can be used to gain further insights into what causes biases and errors in its OA

527 predictions. Compared to ORACLE (Tsimpidi et al., 2016), ORACLE 2-D tends to produce

528 higher fresh SOA concentrations and slightly lower aged SOA concentrations. However, this

529 discrepancy may be partially due to the fact that in ORACLE fresh SOA is assumed to

530 correspond only to first generation oxidation products, while in ORACLE 2-D fresh SOA is

531 defined based on the O:C ratio, and includes higher generation oxidation products as well.

532 Overall, the simulated average total SOA concentrations in ORACLE 2-D (2.59 μg m^{-3}) are

533 higher than ORACLE (1.91 μg m^{-3}) reducing the gap with the corresponding AMS OOA (2.78

534 μg m^{-3}).

535

536 **5.2 O:C ratio**

537 The simulated O:C ratio of total OA and SOA is compared against observed O:C of OA

538 and OOA from 30 and 57 field campaigns, respectively, performed during the period 2001–2010

539 in the Northern Hemisphere (Tables 5, 6). Given that global models, including EMAC,

540 underestimate concentrations of POA and SOA over urban locations (Tsigaridis et al., 2014;

541 Tsimpidi et al., 2016), AMS data from these locations is not included for the statistical

542 evaluation of the calculated O:C (Figure 9, Tables 7, 8). In fact, the model tends to overestimate

543 the O:C of total OA compared to observations from urban locations (e.g., Mexico City,

544 Barcelona, New York, Riverside, Paris; Table 5). This overprediction can be attributed to the

545 coarse spatial resolution and the difficulty to represent freshly emitted (or formed) OA on a local

546 scale. On the other hand, the model performs remarkably well in reproducing the O:C ratio of

547 both total OA (NMB=7%, RMSE=0.13) and SOA (NMB=5%, RMSE=0.12) in non-urban areas.

548 The model tends to overestimate the O:C ratio of total OA compared to observations from

549 field campaigns close to the coasts (e.g., western coast of Chile, Mace Head). The model

550 reproduces very well the low O:C ratios of total OA during winter and the higher values during

551 spring and autumn (Table 7). Even if the model substantially underpredicts all types of OA

552 during wintertime, the calculated OA O:C is similar to observations because the relative

553 contribution of each OA compound is captured by the model. The slightly larger underprediction

554 of aged SOA (compared to fresh SOA and POA) during winter results in a small underprediction

555 of total OA O:C (NMB = -7%). This indicates that the missing OA during winter cannot be

556 attributed only to missing POA sources (e.g., residential biofuel use) but also to missing SOA

557 formation pathways (e.g., multiphase oxidation). On the other hand, it overestimates the O:C of

558 total OA during summer (MB=0.14). Field campaigns conducted during the summer months

559 provide O:C of total OA with surprisingly low O:C values for this time of the year (0.3-0.4)

560 which are not captured by the model. Overall, the O:C of total OA is slightly overestimated by

561 the model (MB=0.04).

562 Simulated O:C of SOA is relatively high (0.5-0.7) at most observational sites, which

563 agrees well with measurements. The model also captures the very high O:C values (larger than

564 0.7) observed over very remote areas (e.g., Okinawa, Finokalia). On the other hand, low O:C

565 ratios (lower than 0.5), reported by a few field campaigns, are overestimated by the model (Duke

566 forest, Rhine Valley, Jiaxing). Remarkably, the model performance during winter is unbiased for

567 the O:C ratio of SOA (Table 8). This is in contrast to its inability to reproduce SOA

568 concentrations during winter (Tsimpidi et al., 2016). During the other seasons the model slightly

569 overestimates the O:C ratio of SOA with an MB ranging from 0.02 (during spring) to 0.07

570 (during summer and autumn).

Furthermore, the O:C ratios of total OA presented here can be used to calculate the OM/OC based on Eqs. 6 and 10. The average calculated OM/OC is 1.8, compared to the observed 1.75. This is also in accordance with the OM/OC value of 1.84 reported by Canagaratna et al. (2015) obtained from a large dataset of chamber and ambient OA measurements. The calculated OM/OC ranges from 1.6 during winter to 2 during autumn, while the observed O:C ranges from 1.6 during summer to 1.8 during spring and autumn.

6. Conclusions

The ORACLE module for the description of OA composition and evolution in the atmosphere (Tsimpidi et al., 2014) has been extended to simultaneously simulate the volatility and the oxygen content of OA that results from atmospheric aging. Similar to ORACLE v1.0, the new version is implemented in the EMAC CCM, and considers the formation of OA from the emissions and chemical aging of LVOCs, SVOCs and IVOCs from fossil fuel, biofuel and biomass burning related sources, as well as from the oxidation of anthropogenic and biogenic VOC precursors. The updated ORACLE module employs the 2-D VBS framework that uses logarithmically spaced effective saturation concentration bins to describe the volatility of organic compounds, and linearly spaced oxygen per carbon ratio bins to describe their oxygenation state.

The simulated concentrations of OA and its components (i.e., POA and SOA) are similar to ORACLE v1.0 with relatively high concentrations over the industrialized areas in the Northern Hemisphere and the biomass burning areas in the tropics. The tropospheric burdens of POA and SOA are calculated to be 0.25 and 3.05 Tg respectively, the latter being higher than with ORACLE v1.0. The new ORACLE 2-D module additionally allows calculation of the oxidation state of OA (in terms of O:C), and therefore, its classification into fresh SOA (with O:C lower than 0.6) and aged SOA (with O:C higher than 0.6). O:C is calculated to be relatively low close to source regions and at high latitudes. The predicted O:C ratio is as low as 0.3 over the boreal forests, 0.3-0.4 close to the anthropogenic sources in the Northern Hemisphere, 0.5 over the tropical forests and higher than 0.6 downwind of source areas and at altitudes aloft. Accordingly, fresh SOA concentrations are higher close to sources while aged SOA increases as the air masses are transported away from the sources and to higher altitudes. The estimated tropospheric burden of fresh SOA is 1.26 Tg and of aged SOA 1.79 Tg. The analysis of model

602 results regarding the distribution of OA in the 2-D space of volatility and oxygen content showed

603 that half of OA has $C^* = 1$ µg m^{-3} over both anthropogenic areas (e.g., Europe) and tropical

604 forests (e.g., Amazon). Furthermore, over Europe OA compounds are more strongly oxidized

605 than over the Amazon, and consist of 40% fresh OA and 30% aged SOA (compared to 55% and

606 15%, respectively, over the Amazon). The remainder 30% in both areas consists of POA or very

607 low oxidized material with O:C≤0.2.

608 The simulated OA components (POA, fresh, aged and total SOA) have been compared

609 with observed subtypes of OA (sum of HOA and BBOA, SVOOA, LVOOA and OOA) derived

610 from AMS factor analysis results from 61 field campaigns, performed during the period 2001–

611 2010 over urban-downwind and rural environments in the Northern Hemisphere. The model

612 reproduces the POA concentrations over both types of environment with low bias. While the

613 model appears to capture the fresh SOA concentrations reasonably well, it underestimates the

614 concentrations of aged SOA, resulting in an overall underprediction of total SOA. While this

615 aged SOA underestimation is evident throughout the year, it is more pronounced during winter.

616 The underestimation of aged SOA by the model emphasizes the need to better describe chemical

617 aging processes and further explore the effect of ELVOCs on the formation of SOA.

618 Furthermore, the model realistically reproduces the observed O:C ratio of total OA over urban-

619 downwind and rural areas. It adequately captures the low values during winter and the higher

620 during spring and autumn, however, it overestimates the O:C of total OA during summer. In

621 addition, the model slightly overestimates the O:C ratio of total OOA (NMB=5%), except during

622 winter when modeled OOA O:C is unbiased.

623 ORACLE 2-D is a flexible module that efficiently describes the organic aerosol

624 composition and evolution in the atmosphere by simulating the changes in OA volatility and

625 oxygen content throughout its lifetime in the atmosphere. The ability of ORACLE 2-D to

626 simulate the degree of OA oxidation can help determine the changing OA hygroscopicity during

627 atmospheric aging. ORACLE 2-D can potentially provide valuable insights into the composition

628 and reactivity of OA and the physicochemical evolution during atmospheric transport of OA,

629 which can help reduce aerosol-related uncertainties that persist in global atmospheric chemistry

630 and climate modeling.

631

632

Code and Data Availability

The complete ORACLE 2-D code can be obtained by applying for an EMAC license or upon request by emailing the first author. To use ORACLE 2-D as part of EMAC, please first apply for an ECHAM5 and a MESSy license. The GCM ECHAM5 has been developed at the Max Planck Institute for Meteorology in Hamburg (see: www.mpimet.mpg.de/en/wissenschaft/modelle/echam/echam5.html). The Modular Earth Submodel System (MESSy) is developed and applied by a consortium of institutions, initiated by the Max Planck Institute for Chemistry. The usage of MESSy and access to the source code is licensed to all affiliates of institutions that are members of the MESSy Consortium. Institutions can be a member of the MESSy Consortium by signing the MESSy Memorandum of Understanding. More information can be found on the MESSy Consortium Website (www.messy-interface.org). The measurement data used for the evaluation of the model can be found in Tables 5 and 6 of this manuscript and Tables S6 and S7 in the supplement of Tsimpidi et al. (2016) (available online at https://doi.org/10.5194/acp-16-8939-2016-supplement).

Acknowledgements

A.P. Tsimpidi acknowledges support from a DFG individual grand programme (project reference TS 335/2-1) and V.A. Karydis acknowledges support from a FP7 Marie Curie Career Integration Grant (project reference 618349).

References

Ahmadov, R., McKeen, S. A., Robinson, A. L., Bahreini, R., Middlebrook, A. M., de Gouw, J. A., Meagher, J., Hsie, E. Y., Edgerton, E., Shaw, S., and Trainer, M.: A volatility basis set model for summertime secondary organic aerosols over the eastern United States in 2006, J. Geophys. Res. Atmos., 117, 10.1029/2011jd016831, 2012.

Aiken, A. C., Decarlo, P. F., Kroll, J. H., Worsnop, D. R., Huffman, J. A., Docherty, K. S., Ulbrich, I. M., Mohr, C., Kimmel, J. R., Sueper, D., Sun, Y., Zhang, Q., Trimborn, A., Northway, M., Ziemann, P. J., Canagaratna, M. R., Onasch, T. B., Alfarra, M. R., Prevot, A. S. H., Dommen, J., Duplissy, J., Metzger, A., Baltensperger, U., and Jimenez, J. L.: O/C and OM/OC ratios of primary, secondary, and ambient organic aerosols with high-resolution time-of-flight aerosol mass spectrometry, Environmen. Sci. & Technol., 42, 4478-4485, 2008.

Allan, J. D., Williams, P. I., Morgan, W. T., Martin, C. L., Flynn, M. J., Lee, J., Nemitz, E., Phillips, G. J., Gallagher, M. W., and Coe, H.: Contributions from transport, solid fuel

burning and cooking to primary organic aerosols in two UK cities, Atmospheric Chemistry and Physics, 10, 647-668, 10.5194/acp-10-647-2010, 2010.

Athanasopoulou, E., Vogel, H., Vogel, B., Tsimpidi, A. P., Pandis, S. N., Knote, C., and Fountoukis, C.: Modeling the meteorological and chemical effects of secondary organic aerosols during an EUCAARI campaign, Atmos. Chem. Phys., 13, 625-645, 2013.

Bacer, S., Sullivan, S. C., Karydis, V. A., Barahona, D., Krämer, M., Nenes, A., Tost, H., Tsimpidi, A. P., Lelieveld, J., and Pozzer, A.: Implementation of a comprehensive ice crystal formation parameterization for cirrus and mixed-phase clouds into the EMAC model (based on MESSy 2.53), Geosci. Model Dev. Discuss., 2018, 1-26, 10.5194/gmd-2018-62, 2018.

Canagaratna, M. R., Jimenez, J. L., Kroll, J. H., Chen, Q., Kessler, S. H., Massoli, P., Ruiz, L. H., Fortner, E., Williams, L. R., Wilson, K. R., Surratt, J. D., Donahue, N. M., Jayne, J. T., and Worsnop, D. R.: Elemental ratio measurements of organic compounds using aerosol mass spectrometry: characterization, improved calibration, and implications, Atmospheric Chemistry and Physics, 15, 253-272, 10.5194/acp-15-253-2015, 2015.

Carbone, S., Aurela, M., Saarnio, K., Saarikoski, S., Timonen, H., Frey, A., Sueper, D., Ulbrich, I. M., Jimenez, J. L., Kulmala, M., Worsnop, D. R., and Hillamo, R. E.: Wintertime Aerosol Chemistry in Sub-Arctic Urban Air, Aerosol Science and Technology, 48, 313-323, 10.1080/02786826.2013.875115, 2014.

Chacon-Madrid, H. J., Henry, K. M., and Donahue, N. M.: Photo-oxidation of pinonaldehyde at low NOx: from chemistry to organic aerosol formation, Atmospheric Chemistry and Physics, 13, 3227-3236, 10.5194/acp-13-3227-2013, 2013.

Chang, R. Y. W., Slowik, J. G., Shantz, N. C., Vlasenko, A., Liggio, J., Sjostedt, S. J., Leaitch, W. R., and Abbatt, J. P. D.: The hygroscopicity parameter (kappa) of ambient organic aerosol at a field site subject to biogenic and anthropogenic influences: relationship to degree of aerosol oxidation, Atmospheric Chemistry and Physics, 10, 5047-5064, 10.5194/acp-10-5047-2010, 2010.

Ciarelli, G., El Haddad, I., Bruns, E., Aksoyoglu, S., Mohler, O., Baltensperger, U., and Prevot, A. S. H.: Constraining a hybrid volatility basis-set model for aging of wood-burning emissions using smog chamber experiments: a box-model study based on the VBS scheme of the CAMx model (v5.40), Geoscientific Model Development, 10, 2303-2320, 10.5194/gmd-10-2303-2017, 2017.

Crippa, M., El Haddad, I., Slowik, J. G., DeCarlo, P. F., Mohr, C., Heringa, M. F., Chirico, R., Marchand, N., Sciare, J., Baltensperger, U., and Prevot, A. S. H.: Identification of marine and continental aerosol sources in Paris using high resolution aerosol mass spectrometry, Journal of Geophysical Research-Atmospheres, 118, 1950-1963, 10.1002/jgrd.50151, 2013.

Docherty, K. S., Aiken, A. C., Huffman, J. A., Ulbrich, I. M., DeCarlo, P. F., Sueper, D., Worsnop, D. R., Snyder, D. C., Peltier, R. E., Weber, R. J., Grover, B. D., Eatough, D. J., Williams, B. J., Goldstein, A. H., Ziemann, P. J., and Jimenez, J. L.: The 2005 Study of Organic Aerosols at Riverside (SOAR-1): instrumental intercomparisons and fine particle composition, Atmospheric Chemistry and Physics, 11, 12387-12420, 10.5194/acp-11-12387-2011, 2011.

Donahue, N. M., Robinson, A. L., Stanier, C. O., and Pandis, S. N.: Coupled partitioning, dilution, and chemical aging of semivolatile organics, Environ. Sci. Technol., 40, 2635-2643, 2006.

Donahue, N. M., Epstein, S. A., Pandis, S. N., and Robinson, A. L.: A two-dimensional volatility basis set: 1. organic-aerosol mixing thermodynamics, Atmos. Chem. and Phys., 11, 3303-3318, 2011.

Ehn, M., Thornton, J. A., Kleist, E., Sipila, M., Junninen, H., Pullinen, I., Springer, M., Rubach, F., Tillmann, R., Lee, B., Lopez-Hilfiker, F., Andres, S., Acir, I.-H., Rissanen, M., Jokinen, T., Schobesberger, S., Kangasluoma, J., Kontkanen, J., Nieminen, T., Kurten, T., Nielsen, L. B., Jorgensen, S., Kjaergaard, H. G., Canagaratna, M., Maso, M. D., Berndt, T., Petaja, T., Wahner, A., Kerminen, V.-M., Kulmala, M., Worsnop, D. R., Wildt, J., and Mentel, T. F.: A large source of low-volatility secondary organic aerosol, Nature, 506, doi: 10.1038/nature13032, 2014.

Fountoukis, C., Megaritis, A. G., Skyllakou, K., Charalampidis, P. E., Pilinis, C., van der Gon, H., Crippa, M., Canonaco, F., Mohr, C., Prevot, A. S. H., Allan, J. D., Poulain, L., Petaja, T., Tiitta, P., Carbone, S., Kiendler-Scharr, A., Nemitz, E., O'Dowd, C., Swietlicki, E., and Pandis, S. N.: Organic aerosol concentration and composition over Europe: insights from comparison of regional model predictions with aerosol mass spectrometer factor analysis, Atmospheric Chemistry and Physics, 14, 9061-9076, 10.5194/acp-14-9061-2014, 2014.

Gao, C. Y., Tsigaridis, K., and Bauer, S. E.: MATRIX-VBS (v1.0): implementing an evolving organic aerosol volatility in an aerosol microphysics model, Geoscientific Model Development, 10, 751-764, 10.5194/gmd-10-751-2017, 2017.

Ge, X. L., Setyan, A., Sun, Y. L., and Zhang, Q.: Primary and secondary organic aerosols in Fresno, California during wintertime: Results from high resolution aerosol mass spectrometry, Journal of Geophysical Research-Atmospheres, 117, 10.1029/2012jd018026, 2012.

Gong, Z. H., Lan, Z. J., Xue, L., Zeng, L. W., He, L. Y., and Huang, X. F.: Characterization of submicron aerosols in the urban outflow of the central Pearl River Delta region of China, Frontiers of Environmental Science & Engineering, 6, 725-733, 10.1007/s11783-012-0441-8, 2012.

Guo, H. Y., Liu, J. M., Froyd, K. D., Roberts, J. M., Veres, P. R., Hayes, P. L., Jimenez, J. L., Nenes, A., and Weber, R. J.: Fine particle pH and gas-particle phase partitioning of inorganic species in Pasadena, California, during the 2010 CalNex campaign, Atmospheric Chemistry and Physics, 17, 5703-5719, 10.5194/acp-17-5703-2017, 2017.

Hawkins, L. N., Russell, L. M., Covert, D. S., Quinn, P. K., and Bates, T. S.: Carboxylic acids, sulfates, and organosulfates in processed continental organic aerosol over the southeast Pacific Ocean during VOCALS-REx 2008, Journal of Geophysical Research-Atmospheres, 115, 10.1029/2009jd013276, 2010.

Hayes, P. L., Ortega, A. M., Cubison, M. J., Froyd, K. D., Zhao, Y., Cliff, S. S., Hu, W. W., Toohey, D. W., Flynn, J. H., Lefer, B. L., Grossberg, N., Alvarez, S., Rappenglueck, B., Taylor, J. W., Allan, J. D., Holloway, J. S., Gilman, J. B., Kuster, W. C., De Gouw, J. A., Massoli, P., Zhang, X., Liu, J., Weber, R. J., Corrigan, A. L., Russell, L. M., Isaacman, G., Worton, D. R., Kreisberg, N. M., Goldstein, A. H., Thalman, R., Waxman, E. M., Volkamer, R., Lin, Y. H., Surratt, J. D., Kleindienst, T. E., Offenberg, J. H., Dusanter, S., Griffith, S., Stevens, P. S., Brioude, J., Angevine, W. M., and Jimenez, J. L.: Organic aerosol composition and sources in Pasadena, California, during the 2010 CalNex campaign, Journal of Geophysical Research-Atmospheres, 118, 9233-9257, 10.1002/jgrd.50530, 2013.

He, L. Y., Huang, X. F., Xue, L., Hu, M., Lin, Y., Zheng, J., Zhang, R. Y., and Zhang, Y. H.: Submicron aerosol analysis and organic source apportionment in an urban atmosphere in

Pearl River Delta of China using high-resolution aerosol mass spectrometry, Journal of Geophysical Research-Atmospheres, 116, 10.1029/2010jd014566, 2011.

Hodzic, A., Kasibhatla, P. S., Jo, D. S., Cappa, C. D., Jimenez, J. L., Madronich, S., and Park, R. J.: Rethinking the global secondary organic aerosol (SOA) budget: stronger production, faster removal, shorter lifetime, Atmos. Chem. Phys., 16, 7917-7941, 10.5194/acp-16-7917-2016, 2016.

Holzinger, R., Kasper-Giebl, A., Staudinger, M., Schauer, G., and Rockmann, T.: Analysis of the chemical composition of organic aerosol at the Mt. Sonnblick observatory using a novel high mass resolution thermal-desorption proton-transfer-reaction mass-spectrometer (hr-TD-PTR-MS), Atmospheric Chemistry and Physics, 10, 10111-10128, 10.5194/acp-10-10111-2010, 2010.

Hu, W. W., Hu, M., Hu, W., Jimenez, J. L., Yuan, B., Chen, W. T., Wang, M., Wu, Y. S., Chen, C., Wang, Z. B., Peng, J. F., Zeng, L. M., and Shao, M.: Chemical composition, sources, and aging process of submicron aerosols in Beijing: Contrast between summer and winter, Journal of Geophysical Research-Atmospheres, 121, 1955-1977, 10.1002/2015jd024020, 2016.

Huang, X. F., He, L. Y., Hu, M., Canagaratna, M. R., Sun, Y., Zhang, Q., Zhu, T., Xue, L., Zeng, L. W., Liu, X. G., Zhang, Y. H., Jayne, J. T., Ng, N. L., and Worsnop, D. R.: Highly time-resolved chemical characterization of atmospheric submicron particles during 2008 Beijing Olympic Games using an Aerodyne High-Resolution Aerosol Mass Spectrometer, Atmospheric Chemistry and Physics, 10, 8933-8945, 10.5194/acp-10-8933-2010, 2010.

Huang, X. F., He, L. Y., Hu, M., Canagaratna, M. R., Kroll, J. H., Ng, N. L., Zhang, Y. H., Lin, Y., Xue, L., Sun, T. L., Liu, X. G., Shao, M., Jayne, J. T., and Worsnop, D. R.: Characterization of submicron aerosols at a rural site in Pearl River Delta of China using an Aerodyne High-Resolution Aerosol Mass Spectrometer, Atmospheric Chemistry and Physics, 11, 1865-1877, 10.5194/acp-11-1865-2011, 2011.

Huang, X. F., Xue, L., Tian, X. D., Shao, W. W., Sun, T. L., Gong, Z. H., Ju, W. W., Jiang, B., Hu, M., and He, L. Y.: Highly time-resolved carbonaceous aerosol characterization in Yangtze River Delta of China: Composition, mixing state and secondary formation, Atmospheric Environment, 64, 200-207, 10.1016/j.atmosenv.2012.09.059, 2013.

Jathar, S. H., Farina, S. C., Robinson, A. L., and Adams, P. J.: The influence of semi-volatile and reactive primary emissions on the abundance and properties of global organic aerosol, Atmos. Chem. Phys., 11, 7727-7746, 2011.

Jathar, S. H., Mahmud, A., Barsanti, K. C., Asher, W. E., Pankow, J. F., and Kleeman, M. J.: Water uptake by organic aerosol and its influence on gas/particle partitioning of secondary organic aerosol in the United States, Atmospheric Environment, 129, 142-154, 10.1016/j.atmosenv.2016.01.001, 2016.

Jo, D. S., Park, R. J., Kim, M. J., and Spracklen, D. V.: Effects of chemical aging on global secondary organic aerosol using the volatility basis set approach, Atmos. Environ., 81, 230-244, 2013.

Jöckel, P., Tost, H., Pozzer, A., Bruehl, C., Buchholz, J., Ganzeveld, L., Hoor, P., Kerkweg, A., Lawrence, M. G., Sander, R., Steil, B., Stiller, G., Tanarhte, M., Taraborrelli, D., Van Aardenne, J., and Lelieveld, J.: The atmospheric chemistry general circulation model ECHAM5/MESSy1: consistent simulation of ozone from the surface to the mesosphere, Atmos. Chem. Phys., 6, 5067-5104, 2006.

Karydis, V. A., Tsimpidi, A. P., Pozzer, A., Astitha, M., and Lelieveld, J.: Effects of mineral dust on global atmospheric nitrate concentrations, Atmos. Chem. Phys., 16, 1491-1509, 10.5194/acp-16-1491-2016, 2016.

Karydis, V. A., Tsimpidi, A. P., Bacer, S., Pozzer, A., Nenes, A., and Lelieveld, J.: Global impact of mineral dust on cloud droplet number concentration, Atmospheric Chemistry and Physics, 17, 5601-5621, 10.5194/acp-17-5601-2017, 2017.

Kerkweg, A., Buchholz, J., Ganzeveld, L., Pozzer, A., Tost, H., and Jöckel, P.: Technical Note: An implementation of the dry removal processes DRY DEPosition and SEDImentation in the Modular Earth Submodel System (MESSy), Atmos. Chem. Phys., 6, 4617-4632, 2006a.

Kerkweg, A., Sander, R., Tost, H., and Jöckel, P.: Technical note: Implementation of prescribed (OFFLEM), calculated (ONLEM), and pseudo-emissions (TNUDGE) of chemical species in the Modular Earth Submodel System (MESSy), Atmos. Chem. Phys., 6, 3603-3609, 10.5194/acp-6-3603-2006, 2006b.

Koo, B., Knipping, E., and Yarwood, G.: 1.5-Dimensional volatility basis set approach for modeling organic aerosol in CAMx and CMAQ, Atmospheric Environment, 95, 158-164, 10.1016/j.atmosenv.2014.06.031, 2014.

Kuwata, M., and Lee, W. C.: 1-octanol-water partitioning as a classifier of water soluble organic matters: Implication for solubility distribution, Aerosol Science and Technology, 51, 602-613, 10.1080/02786826.2017.1283004, 2017.

Lambe, A. T., Onasch, T. B., Massoli, P., Croasdale, D. R., Wright, J. P., Ahern, A. T., Williams, L. R., Worsnop, D. R., Brune, W. H., and Davidovits, P.: Laboratory studies of the chemical composition and cloud condensation nuclei (CCN) activity of secondary organic aerosol (SOA) and oxidized primary organic aerosol (OPOA), Atmospheric Chemistry and Physics, 11, 8913-8928, 10.5194/acp-11-8913-2011, 2011.

Lane, T. E., Donahue, N. M., and Pandis, S. N.: Simulating secondary organic aerosol formation using the volatility basis-set approach in a chemical transport model, Atmos. Environ., 42, 7439-7451, 2008.

Lauer, A., Eyring, V., Hendricks, J., Joeckel, P., and Lohmann, U.: Global model simulations of the impact of ocean-going ships on aerosols, clouds, and the radiation budget, Atmos. Chem. Phys., 7, 5061-5079, 2007.

Liggio, J., Li, S. M., Vlasenko, A., Sjostedt, S., Chang, R., Shantz, N., Abbatt, J., Slowik, J. G., Bottenheim, J. W., Brickell, P. C., Stroud, C., and Leaitch, W. R.: Primary and secondary organic aerosols in urban air masses intercepted at a rural site, Journal of Geophysical Research-Atmospheres, 115, 10.1029/2010jd014426, 2010.

Martin, S. T., Andreae, M. O., Althausen, D., Artaxo, P., Baars, H., Borrmann, S., Chen, Q., Farmer, D. K., Guenther, A., Gunthe, S. S., Jimenez, J. L., Karl, T., Longo, K., Manzi, A., Muller, T., Pauliquevis, T., Petters, M. D., Prenni, A. J., Poschl, U., Rizzo, L. V., Schneider, J., Smith, J. N., Swietlicki, E., Tota, J., Wang, J., Wiedensohler, A., and Zorn, S. R.: An overview of the Amazonian Aerosol Characterization Experiment 2008 (AMAZE-08), Atmospheric Chemistry and Physics, 10, 11415-11438, 10.5194/acp-10-11415-2010, 2010.

May, A. A., Levin, E. J. T., Hennigan, C. J., Riipinen, I., Lee, T., Collett, J. L., Jimenez, J. L., Kreidenweis, S. M., and Robinson, A. L.: Gas-particle partitioning of primary organic aerosol emissions: 3. Biomass burning, Journal of Geophysical Research-Atmospheres, 118, 11327-11338, 10.1002/jgrd.50828, 2013.

Mohr, C., DeCarlo, P. F., Heringa, M. F., Chirico, R., Slowik, J. G., Richter, R., Reche, C., Alastuey, A., Querol, X., Seco, R., Penuelas, J., Jimenez, J. L., Crippa, M., Zimmermann, R.,

Baltensperger, U., and Prevot, A. S. H.: Identification and quantification of organic aerosol from cooking and other sources in Barcelona using aerosol mass spectrometer data, Atmospheric Chemistry and Physics, 12, 1649-1665, 10.5194/acp-12-1649-2012, 2012.

Murphy, B. N., and Pandis, S. N.: Simulating the formation of semivolatile primary and secondary organic aerosol in a regional chemical transport model, Environ. Sci. Technol., 43, 4722-4728, 2009.

Murphy, B. N., Donahue, N. M., Fountoukis, C., and Pandis, S. N.: Simulating the oxygen content of ambient organic aerosol with the 2D volatility basis set, Atmos. Chem. Phys., 11, 7859-7873, 2011.

Murphy, B. N., Donahue, N. M., Fountoukis, C., Dall'Osto, M., O'Dowd, C., Kiendler-Scharr, A., and Pandis, S. N.: Functionalization and fragmentation during ambient organic aerosol aging: application of the 2-D volatility basis set to field studies, Atmospheric Chemistry and Physics, 12, 10797-10816, 10.5194/acp-12-10797-2012, 2012.

Napier, W. J., Ensberg, J. J., and Seinfeld, J. H.: Insight into the numerical challenges of implementing 2-dimensional SOA models in atmospheric chemical transport models, Atmospheric Environment, 96, 331-344, 10.1016/j.atmosenv.2014.07.048, 2014.

Ng, N. L., Canagaratna, M. R., Zhang, Q., Jimenez, J. L., Tian, J., Ulbrich, I. M., Kroll, J. H., Docherty, K. S., Chhabra, P. S., Bahreini, R., Murphy, S. M., Seinfeld, J. H., Hildebrandt, L., Donahue, N. M., DeCarlo, P. F., Lanz, V. A., Prévôt, A. S. H., Dinar, E., Rudich, Y., and Worsnop, D. R.: Organic aerosol components observed in Northern Hemispheric datasets from Aerosol Mass Spectrometry, Atmos. Chem. Phys., 10, 4625-4641, 10.5194/acp-10-4625-2010, 2010.

Paciga, A., Karnezi, E., Kostenidou, E., Hildebrandt, L., Psichoudaki, M., Engelhart, G. J., Lee, B. H., Crippa, M., Prevot, A. S. H., Baltensperger, U., and Pandis, S. N.: Volatility of organic aerosol and its components in the megacity of Paris, Atmospheric Chemistry and Physics, 16, 2013-2023, 10.5194/acp-16-2013-2016, 2016.

Pankow, J. F., and Asher, W. E.: SIMPOL.1: a simple group contribution method for predicting vapor pressures and enthalpies of vaporization of multifunctional organic compounds, Atmospheric Chemistry and Physics, 8, 2773-2796, 10.5194/acp-8-2773-2008, 2008.

Pathak, R. K., Presto, A. A., Lane, T. E., Stanier, C. O., Donahue, N. M., and Pandis, S. N.: Ozonolysis of alpha-pinene: parameterization of secondary organic aerosol mass fraction, Atmospheric Chemistry and Physics, 7, 3811-3821, 2007.

Pozzer, A., Zimmermann, P., Doering, U. M., van Aardenne, J., Tost, H., Dentener, F., Janssens-Maenhout, G., and Lelieveld, J.: Effects of business-as-usual anthropogenic emissions on air quality, Atmos. Chem. Phys., 12, 6915-6937, 10.5194/acp-12-6915-2012, 2012.

Pringle, K. J., Tost, H., Message, S., Steil, B., Giannadaki, D., Nenes, A., Fountoukis, C., Stier, P., Vignati, E., and Leieved, J.: Description and evaluation of GMXe: a new aerosol submodel for global simulations (v1), Geoscientific Model Development, 3, 391-412, 2010.

Pye, H. O. T., and Seinfeld, J. H.: A global perspective on aerosol from low-volatility organic compounds, Atmos. Chem. Phys., 10, 4377-4401, 2010.

Robinson, A. L., Donahue, N. M., Shrivastava, M. K., Weitkamp, E. A., Sage, A. M., Grieshop, A. P., Lane, T. E., Pierce, J. R., and Pandis, S. N.: Rethinking organic aerosols: Semivolatile emissions and photochemical aging, Science, 315, 1259-1262, 2007.

Roeckner, E., Brokopf, R., Esch, M., Giorgetta, M., Hagemann, S., Kornblueh, L., Manzini, E., Schlese, U., and Schulzweida, U.: Sensitivity of simulated climate to horizontal and vertical

resolution in the ECHAM5 atmosphere model, Journal of Climate, 19, 3771-3791, 10.1175/jcli3824.1, 2006.

Saarikoski, S., Carbone, S., Decesari, S., Giulianelli, L., Angelini, F., Canagaratna, M., Ng, N. L., Trimborn, A., Facchini, M. C., Fuzzi, S., Hillamo, R., and Worsnop, D.: Chemical characterization of springtime submicrometer aerosol in Po Valley, Italy, Atmospheric Chemistry and Physics, 12, 8401-8421, 10.5194/acp-12-8401-2012, 2012.

Sander, R., Baumgaertner, A., Gromov, S., Harder, H., Joeckel, P., Kerkweg, A., Kubistin, D., Regelin, E., Riede, H., Sandu, A., Taraborrelli, D., Tost, H., and Xie, Z. Q.: The atmospheric chemistry box model CAABA/MECCA-3.0, Geoscientific Model Development, 4, 373-380, 2011.

Shiraiwa, M., Berkemeier, T., Schilling-Fahnestock, K. A., Seinfeld, J. H., and Poschl, U.: Molecular corridors and kinetic regimes in the multiphase chemical evolution of secondary organic aerosol, Atmospheric Chemistry and Physics, 14, 8323-8341, 10.5194/acp-14-8323-2014, 2014.

Shiraiwa, M., Li, Y., Tsimpidi, A. P., Karydis, V. A., Berkemeier, T., Pandis, S. N., Lelieveld, J., Koop, T., and Poschl, U.: Global distribution of particle phase state in atmospheric secondary organic aerosols, Nature Communications, 8, 10.1038/ncomms15002, 2017.

Sun, Y., Zhang, Q., Macdonald, A. M., Hayden, K., Li, S. M., Liggio, J., Liu, P. S. K., Anlauf, K. G., Leaitch, W. R., Steffen, A., Cubison, M., Worsnop, D. R., van Donkelaar, A., and Martin, R. V.: Size-resolved aerosol chemistry on Whistler Mountain, Canada with a high-resolution aerosol mass spectrometer during INTEX-B, Atmospheric Chemistry and Physics, 9, 3095-3111, 10.5194/acp-9-3095-2009, 2009.

Sun, Y. L., Zhang, Q., Schwab, J. J., Demerjian, K. L., Chen, W. N., Bae, M. S., Hung, H. M., Hogrefe, O., Frank, B., Rattigan, O. V., and Lin, Y. C.: Characterization of the sources and processes of organic and inorganic aerosols in New York city with a high-resolution time-of-flight aerosol mass apectrometer, Atmospheric Chemistry and Physics, 11, 1581-1602, 10.5194/acp-11-1581-2011, 2011.

Thomson, A. M., Calvin, K. V., Smith, S. J., Kyle, G. P., Volke, A., Patel, P., Delgado-Arias, S., Bond-Lamberty, B., Wise, M. A., Clarke, L. E., and Edmonds, J. A.: RCP4.5: a pathway for stabilization of radiative forcing by 2100, Climatic Change, 109, 77-94, 2011.

Timonen, H., Carbone, S., Aurela, M., Saarnio, K., Saarikoski, S., Ng, N. L., Canagaratna, M. R., Kulmala, M., Kerminen, V. M., Worsnop, D. R., and Hillamo, R.: Characteristics, sources and water-solubility of ambient submicron organic aerosol in springtime in Helsinki, Finland, Journal of Aerosol Science, 56, 61-77, 10.1016/j.jaerosci.2012.06.005, 2013.

Tost, H., Jockel, P. J., Kerkweg, A., Sander, R., and Lelieveld, J.: Technical note: A new comprehensive SCAVenging submodel for global atmospheric chemistry modelling, Atmos. Chem. Phys., 6, 565-574, 2006.

Trail, M., Tsimpidi, A. P., Liu, P., Tsigaridis, K., Hu, Y., Nenes, A., and Russell, A. G.: Downscaling a global climate model to simulate climate change over the US and the implication on regional and urban air quality, Geoscientific Model Development, 6, 1429-1445, 10.5194/gmd-6-1429-2013, 2013.

Trail, M., Tsimpidi, A. P., Liu, P., Tsigaridis, K., Rudokas, J., Miller, P., Nenes, A., Hu, Y., and Russell, A. G.: Sensitivity of air quality to potential future climate change and emissions in the United States and major cities, Atmospheric Environment, 94, 552-563, 10.1016/j.atmosenv.2014.05.079, 2014.

Tsigaridis, K., Daskalakis, N., Kanakidou, M., Adams, P. J., Artaxo, P., Bahadur, R., Balkanski, Y., Bauer, S. E., Bellouin, N., Benedetti, A., Bergman, T., Berntsen, T. K., Beukes, J. P., Bian, H., Carslaw, K. S., Chin, M., Curci, G., Diehl, T., Easter, R. C., Ghan, S. J., Gong, S. L., Hodzic, A., Hoyle, C. R., Iversen, T., Jathar, S., Jimenez, J. L., Kaiser, J. W., Kirkevag, A., Koch, D., Kokkola, H., Lee, Y. H., Lin, G., Liu, X., Luo, G., Ma, X., Mann, G. W., Mihalopoulos, N., Morcrette, J. J., Mueller, J. F., Myhre, G., Myriokefalitakis, S., Ng, N. L., O'Donnell, D., Penner, J. E., Pozzoli, L., Pringle, K. J., Russell, L. M., Schulz, M., Sciare, J., Seland, O., Shindell, D. T., Sillman, S., Skeie, R. B., Spracklen, D., Stavrakou, T., Steenrod, S. D., Takemura, T., Tiitta, P., Tilmes, S., Tost, H., van Noije, T., van Zyl, P. G., von Salzen, K., Yu, F., Wang, Z., Wang, Z., Zaveri, R. A., Zhang, H., Zhang, K., Zhang, Q., and Zhang, X.: The AeroCom evaluation and intercomparison of organic aerosol in global models, Atmospheric Chemistry and Physics, 14, 10845-10895, 10.5194/acp-14-10845-2014, 2014.

Tsimpidi, A. P., Karydis, V. A., Zavala, M., Lei, W., Molina, L., Ulbrich, I. M., Jimenez, J. L., and Pandis, S. N.: Evaluation of the volatility basis-set approach for the simulation of organic aerosol formation in the Mexico City metropolitan area, Atmos. Chem. Phys., 10, 525-546, 2010.

Tsimpidi, A. P., Karydis, V. A., Zavala, M., Lei, W., Bei, N., Molina, L., and Pandis, S. N.: Sources and production of organic aerosol in Mexico City: insights from the combination of a chemical transport model (PMCAMx-2008) and measurements during MILAGRO, Atmos. Chem. Phys., 11, 5153-5168, 2011.

Tsimpidi, A. P., Karydis, V. A., Pozzer, A., Pandis, S. N., and Lelieveld, J.: ORACLE (v1.0): module to simulate the organic aerosol composition and evolution in the atmosphere, Geoscientific Model Development, 7, 3153-3172, 10.5194/gmd-7-3153-2014, 2014.

Tsimpidi, A. P., Karydis, V. A., Pandis, S. N., and Lelieveld, J.: Global combustion sources of organic aerosols: model comparison with 84 AMS factor-analysis data sets, Atmos. Chem. Phys., 16, 8939-8962, 10.5194/acp-16-8939-2016, 2016.

Tsimpidi, A. P., Karydis, V. A., Pandis, S. N., and Lelieveld, J.: Global-scale combustion sources of organic aerosols: sensitivity to formation and removal mechanisms, Atmospheric Chemistry and Physics, 17, 7345-7364, 10.5194/acp-17-7345-2017, 2017.

van der Gon, H., Bergstrom, R., Fountoukis, C., Johansson, C., Pandis, S. N., Simpson, D., and Visschedijk, A. J. H.: Particulate emissions from residential wood combustion in Europe revised estimates and an evaluation, Atmospheric Chemistry and Physics, 15, 6503-6519, 10.5194/acp-15-6503-2015, 2015.

van der Werf, G. R., Randerson, J. T., Giglio, L., Collatz, G. J., Mu, M., Kasibhatla, P. S., Morton, D. C., DeFries, R. S., Jin, Y., and van Leeuwen, T. T.: Global fire emissions and the contribution of deforestation, savanna, forest, agricultural, and peat fires (1997-2009), Atmos. Chem. Phys., 10, 11707-11735, 2010.

Xu, L., Guo, H. Y., Boyd, C. M., Klein, M., Bougiatioti, A., Cerully, K. M., Hite, J. R., Isaacman-VanWertz, G., Kreisberg, N. M., Knote, C., Olson, K., Koss, A., Goldstein, A. H., Hering, S. V., de Gouw, J., Baumann, K., Lee, S. H., Nenes, A., Weber, R. J., and Ng, N. L.: Effects of anthropogenic emissions on aerosol formation from isoprene and monoterpenes in the southeastern United States, Proceedings of the National Academy of Sciences of the United States of America, 112, 37-42, 10.1073/pnas.1417609112, 2015.

Zhang, Q., Jimenez, J. L., Canagaratna, M. R., Allan, J. D., Coe, H., Ulbrich, I., Alfarra, M. R., Takami, A., Middlebrook, A. M., Sun, Y. L., Dzepina, K., Dunlea, E., Docherty, K., DeCarlo, P. F., Salcedo, D., Onasch, T., Jayne, J. T., Miyoshi, T., Shimono, A., Hatakeyama,

984   S., Takegawa, N., Kondo, Y., Schneider, J., Drewnick, F., Borrmann, S., Weimer, S.,
985   Demerjian, K., Williams, P., Bower, K., Bahreini, R., Cottrell, L., Griffin, R. J., Rautiainen,
986   J., Sun, J. Y., Zhang, Y. M., and Worsnop, D. R.: Ubiquity and dominance of oxygenated
987   species in organic aerosols in anthropogenically-influenced Northern Hemisphere
988   midlatitudes, Geophys. Res. Lett., 34, doi: L13801 10.1029/2007gl029979, 2007.
989 Zhao, B., Wang, S. X., Donahue, N. M., Chuang, W. N., Hildebrandt Ruiz, L., Ng, N. L., Wang,
990   Y. J., and Hao, J. M.: Evaluation of One-Dimensional and Two-Dimensional Volatility Basis
991   Sets in Simulating the Aging of Secondary Organic Aerosol with Smog-Chamber
992   Experiments, Environmental Science & Technology, 49, 2245-2254, 10.1021/es5048914,
993   2015.

994
995

996   **Table 1.** Statistical evaluation of EMAC POA against AMS POA (sum of HOA and BBOA)

997   from 61 data sets worldwide during 2001-2010.

998

Site Type	Number of datasets	Mean Observed (μg m^{-3})	Mean Predicted (μg m^{-3})	MAGE (μg m^{-3})	MB (μg m^{-3})	NME (%)	NMB (%)	RMSE (μg m^{-3})
Urban Downwind	15	0.82	0.65	0.39	-0.17	47	-21	0.51
Rural/Remote	46	0.43	0.45	0.38	0.02	88	6	0.50
Season								
Winter	6	1.18	0.72	0.66	-0.45	56	-38	0.78
Spring	30	0.42	0.52	0.40	0.10	95	24	0.50
Summer	14	0.50	0.45	0.30	-0.05	60	-12	0.40
Autumn	11	0.49	0.41	0.28	-0.08	57	-18	0.38
Total	61	0.53	0.50	0.38	-0.03	72	-5	0.50

999
1000

1001   **Table 2.** Statistical evaluation of EMAC SOA against AMS OOA from 61 data sets worldwide

1002   during 2001-2010.

1003

Site Type	Number of datasets	Mean Observed ($\mu g\ m^{-3}$)	Mean Predicted ($\mu g\ m^{-3}$)	MAGE ($\mu g\ m^{-3}$)	MB ($\mu g\ m^{-3}$)	NME (%)	NMB (%)	RMSE ($\mu g\ m^{-3}$)
Urban Downwind	15	2.98	2.76	1.32	-0.22	44	-7	1.82
Rural/Remote	46	2.72	2.53	1.52	-0.18	56	-7	2.11
Season								
Winter	6	2.81	0.67	2.14	-2.14	76	-76	2.52
Spring	30	2.22	2.48	1.05	0.25	47	11	1.44
Summer	14	4.30	3.85	2.23	-0.45	52	-10	2.99
Autumn	11	2.35	2.34	1.29	-0.01	55	0	1.60
Total	61	2.78	2.59	1.47	-0.19	53	-7	2.04

1004
1005
1006

1007   **Table 3.** Statistical evaluation of EMAC aged SOA against AMS LVOOA from 41 data sets

1008   worldwide during 2001-2010.

1009

Site Type	Number of datasets	Mean Observed (μg m^{-3})	Mean Predicted (μg m^{-3})	MAGE (μg m^{-3})	MB (μg m^{-3})	NME (%)	NMB (%)	RMSE (μg m^{-3})
Urban Downwind	8	1.77	0.81	1.26	-0.95	71	-54	1.57
Rural/Remote	33	1.65	0.95	1.18	-0.70	72	-42	1.71
Season								
Winter	3	2.36	0.17	2.19	-2.19	93	-93	2.40
Spring	18	1.06	0.73	0.84	-0.33	79	-32	1.05
Summer	11	2.64	1.46	1.74	-1.18	66	-45	2.47
Autumn	9	1.49	0.92	0.92	-0.57	62	-38	1.14
Total	41	1.68	0.93	1.20	-0.75	72	-45	1.68

1010

1011

1012 **Table 4.** Statistical evaluation of EMAC fresh SOA against AMS SVOOA from 41 data sets

1013 worldwide during 2001-2010.

1014

Site Type	Number of datasets	Mean Observed (μg m^{-3})	Mean Predicted (μg m^{-3})	MAGE (μg m^{-3})	MB (μg m^{-3})	NME (%)	NMB (%)	RMSE (μg m^{-3})
Urban Downwind	8	0.81	1.22	0.75	0.41	92	50	0.98
Rural/Remote	33	1.03	1.35	0.82	0.32	79	31	1.03
Season								
Winter	3	0.87	0.36	0.51	-0.51	59	-59	0.63
Spring	18	0.54	0.88	0.66	0.34	122	64	0.91
Summer	11	1.89	2.22	1.08	0.33	57	17	1.19
Autumn	9	0.83	1.44	0.86	0.61	104	73	1.11
Total	41	0.99	1.32	0.80	0.33	81	34	1.02

1015

1016

Table 5. Worldwide O:C ratio predictions and observations of total OA.

Location	Lat	Lon	Time period	Measured O:C	Simulated O:C	Reference
Riverside, US	33.95	-117.4	14/07/05-13/08/05	0.35	0.57	Docherty et al. (2011)
Mexico City , MX	19.48	-99.15	10/03/06-30/03/06	0.41	0.55	Aiken et al. (2008)
Whistler, CA	50.01	-122.95	19/04/06-16/05/06	0.83	0.57	Sun et al. (2009)
Egbert, CA	44.23	-79.78	11/05/07-15/06/07	0.45	0.53	Liggio et al. (2010)
London, UK	51.53	-0.15	17/10/07-15/11/07	0.27	0.29	Allan et al. (2010)
Manaus, BR	-2.58	-60.2	07/02/08-14/03/08	0.44	0.50	Martin et al. (2010)
Po Valley, IT	44.65	11.62	30/03/08-20/04/08	0.47	0.56	Saarikoski et al. (2012)
Mace Head, IE	53.3	-9.8	16/05/08-13/06/08	0.53	0.65	Murphy et al. (2012)
Cabauw, NL	51.97	4.93	28/04/08-30/05/08	0.54	0.53	Murphy et al. (2012)
Beijing, CN	40.0	116.0	24/07/08-20/09/08	0.33	0.49	Huang et al. (2010)
West coast, CL	-20	-80	21/10/08-30/11/08	0.62	0.89	Hawkins et al. (2010)
Kaiping, CN	22.32	112.53	12/10/08-18/11/08	0.47	0.41	Huang et al. (2011)
Helsinki, FI	60.2	24.95	09/01/09-13/03/09	0.45	0.25	Carbone et al. (2014)
Barcelona, ES	41.39	2.12	25/02/09-26/03/09	0.36	0.50	Mohr et al. (2012)
Mace Head, IE	53.3	-9.8	26/02/09-26/03/09	0.58	0.65	Murphy et al. (2012)
Cabauw, NL	51.97	4.93	25/02/09-25/02/09	0.34	0.32	Murphy et al. (2012)
Helsinki, FI	60.2	24.95	09/04/09-08/05/09	0.51	0.46	Timonen et al. (2013)
Pasadena, US	34.14	-118.12	22/05/09-12/06/09	0.44	0.51	Guo et al. (2017)
Pasadena, US	34.14	-118.12	18/06/09-07/07/09	0.55	0.56	Guo et al. (2017)
New York, US	40.74	-73.92	13/07/09-03/08/09	0.36	0.55	Sun et al. (2011)
Pasadena, US	34.14	-118.12	10/07/09-04/08/09	0.48	0.55	Guo et al. (2017)
Paris, FR	48.83	2.36	01/07/09-31/07/09	0.38	0.54	Crippa et al. (2013)
Alps, AT	47.05	12.95	10/07/09-31/07/09	0.38	0.58	Holzinger et al. (2010)
Shenzhen, CN	22.6	113.9	25/10/09-02/12/09	0.30	0.41	He et al. (2011)
Fresno, US	36.81	-119.78	09/01/10-23/01/10	0.27	0.46	Ge et al. (2012)
Cool, US	38.88	-121.0	02/06/10-28/06/10	0.44	0.51	Xu et al. (2015)
Jiaxing, CN	30.8	120.8	29/06/10-15/07/10	0.28	0.42	Huang et al. (2013)
Guangzhou, CN	22.71	112.93	13/11/10-01/12/10	0.40	0.42	Gong et al. (2012)
Beijing, CN	40.0	116.0	22/11/10-22/12/10	0.32	0.20	Hu et al. (2016)
Jiaxing, CN	30.8	120.8	11/12/10-23/12/10	0.33	0.24	Huang et al. (2013)

1019   **Table 6.** Worldwide O:C ratio predictions and observations of OOA.

Location	Lat	Lon	Time period	Measured O:C	Simulate O:C	Reference
Cheju Island, KR	33.51	126.50	11/04/01-30/04/01	0.84	0.64	Ng et al. (2010)
Manchester, UK	53.5	-2.22	14/06/01-25/06/01	0.81	0.72	Ng et al. (2010)
New York, US	40.74	-73.92	30/06/01-05/08/01	0.59	0.64	Ng et al. (2010)
Vancouver, CA	49.25	-123.13	11/08/01-24/08/01	0.56	0.59	Ng et al. (2010)
Manchester, UK	53.5	-2.22	17/01/02-28/01/02	0.47	0.61	Ng et al. (2010)
Hohenpeissenberg, DE	47.8	11.0	19/05/02-31/05/02	0.50	0.61	Ng et al. (2010)
East coast, US	37.95	-74.3	18/07/02-26/07/02	0.58	0.67	Ng et al. (2010)
Jungfraujoch , CH	46.3	7.6	28/06/02-17/07/02	0.70	0.63	Ng et al. (2010)
East coast, US	37.95	-74.3	29/07/02-10/08/02	0.60	0.70	Ng et al. (2010)
Pittsburgh, US	40.44	-79.94	06/09/02-22/09/02	0.51	0.60	Ng et al. (2010)
Fukue Island , JP	32.69	128.84	18/03/03-16/04/03	0.65	0.67	Ng et al. (2010)
Hyytiala , FI	61.8	24.3	31/03/05-15/04/05	0.47	0.64	Ng et al. (2010)
Boulder, US	40.02	-105.27	07/06/03-20/06/03	0.44	0.60	Ng et al. (2010)
Tokyo , JP	35.67	139.75	23/07/03-14/08/03	0.49	0.70	Ng et al. (2010)
NE London, UK	51.7	0.4	29/07/03-31/08/03	0.48	0.72	Ng et al. (2010)
Okinawa , JP	26.87	128.25	03/10/03-24/12/03	0.82	0.77	Ng et al. (2010)
Tokyo , JP	35.67	139.75	20/01/04-10/02/04	0.56	0.59	Ng et al. (2010)
New York, US	40.74	-73.92	07/01/04-06/02/04	0.45	0.58	Ng et al. (2010)
Norfolk coast, UK	53.0	1.1	25/04/04-26/05/04	0.70	0.69	Ng et al. (2010)
Wiesbaden, DE	50.22	8.45	14/07/04-04/08/04	0.57	0.63	Ng et al. (2010)
Pinnacle Park, US	43.0	-76	14/07/04-05/08/04	0.64	0.61	Ng et al. (2010)
Nova Scotia, CA	43.76	-66.1	07/07/04-14/08/04	0.65	0.68	Ng et al. (2010)
Mainz, DE	49.98	8.23	16/09/04-01/10/04	0.66	0.62	Ng et al. (2010)
Duke Forest, US	35.97	-79.1	13/09/04-21/09/04	0.46	0.60	Ng et al. (2010)
Roveredo, CH	46.23	9.12	01/03/05-15/03/15	0.43	0.58	Ng et al. (2010)
Harkingen, CH	47.32	7.82	12/05/05-30/05/15	0.55	0.63	Ng et al. (2010)
Riverside, US	33.95	-117.4	14/07/05-13/08/05	0.48	0.62	Ng et al. (2010)
Zurich, CH	47.4	8.5	14/07/05-04/08/05	0.51	0.65	Ng et al. (2010)
Thompson, US	43.11	-70.95	09/07/05-15/08/05	0.58	0.62	Ng et al. (2010)
Roveredo, CH	46.23	9.12	25/11/05-15/12/05	0.56	0.56	Ng et al. (2010)
Zurich, CH	47.4	8.5	06/01/06-25/01/06	0.65	0.54	Ng et al. (2010)
Reiden, CH	47.25	7.97	27/01/06-13/02/06	0.64	0.55	Ng et al. (2010)
Mexico City , MX	19.48	-99.15	10/03/06-30/03/06	0.53	0.69	Ng et al. (2010)
Payerne, CH	46.8	6.95	31/05/06-03/07/06	0.59	0.63	Ng et al. (2010)
Beijing, CN	40.0	116.0	09/07/06-21/07/06	0.50	0.65	Ng et al. (2010)
Massongex, CH	46.24	6.14	23/11/06-17/12/06	0.88	0.55	Ng et al. (2010)
Payerne, CH	46.8	6.95	12/01/07-17/02/07	0.50	0.61	Ng et al. (2010)
Rhine valley, CH	46.29	9	16/02/07-22/02/07	0.34	0.57	Ng et al. (2010)
Egbert, CA	44.23	-79.78	14/05/07-15/06/07	0.61	0.64	Ng et al. (2010)
Po Valley, IT	44.65	11.62	30/03/08-20/04/08	0.65	0.65	Saarikoski et al. (2012)
Finokalia , GR	35.33	25.66	08/05/08-04/06/08	0.80	0.73	Murphy et al. (2012)
Jungfraujoch , CH	46.3	7.6	01/05/08-29/05/08	0.70	0.65	Ng et al. (2010)
Beijing, CN	40.0	116.0	24/07/08-20/10/08	0.48	0.63	Huang et al. (2010)
Kaiping, CN	22.32	112.53	12/10/08-18/11/08	0.52	0.57	Huang et al. (2011)
Grenoble, FR	45.18	5.73	14/01/09-30/01/09	0.65	0.53	Ng et al. (2010)
Helsinki, FI	60.2	24.95	09/01/09-13/03/09	0.60	0.54	Carbone et al. (2014)
Barcelona, ES	41.39	2.12	25/02/09-26/03/09	0.58	0.61	Mohr et al. (2012)
Finokalia , GR	35.33	25.66	25/02/09-25/03/09	0.50	0.67	Murphy et al. (2012)
Helsinki, FI	60.2	24.95	09/04/09-08/05/09	0.58	0.63	Timonen et al. (2013)
New York, US	40.74	-73.92	13/07/09-03/08/09	0.50	0.64	Sun et al. (2011)
Shenzhen, CN	22.6	113.9	25/10/09-02/12/09	0.51	0.58	He et al. (2011)
Fresno, US	36.81	-119.78	09/01/10-23/01/10	0.42	0.62	Ge et al. (2012)
Pasadena, US	34.14	-118.12	15/05/10-16/06/10	0.58	0.61	Hayes et al. (2013)
Jiaxing, CN	30.8	120.8	29/06/10-15/07/10	0.41	0.60	Huang et al. (2013)
Guangzhou, CN	22.71	112.93	13/11/10-01/12/10	0.47	0.58	Gong et al. (2012)
Beijing, CN	40.0	116.0	22/11/10-22/12/10	0.53	0.57	Hu et al. (2016)
Jiaxing, CN	30.8	120.8	11/12/10-23/12/10	0.59	0.50	(Huang et al. (2013))

1020   **Table 7.** Statistical evaluation of EMAC O:C ratio of total OA against observations from 18 data

1021   sets worldwide during 2001-2010.

Season	Number of datasets	Mean Observed ($\mu g\ m^{-3}$)	Mean Predicted ($\mu g\ m^{-3}$)	MAGE ($\mu g\ m^{-3}$)	MB ($\mu g\ m^{-3}$)	NME (%)	NMB (%)	RMSE ($\mu g\ m^{-3}$)
Winter	4	0.42	0.35	0.10	-0.07	24	-17	0.12
Spring	8	0.53	0.53	0.09	0.00	16	1	0.11
Summer	4	0.37	0.51	0.14	0.14	38	38	0.15
Autumn	2	0.51	0.65	0.14	0.14	28	28	0.19
Total	18	0.47	0.50	0.11	0.03	23	7	0.13

1022

1023 **Table 8.** Statistical evaluation of EMAC O:C ratio of OOA against observations from 32 data

1024 sets worldwide during 2001-2010.

Season	Number of datasets	Mean Observed ($\mu g\ m^{-3}$)	Mean Predicted ($\mu g\ m^{-3}$)	MAGE ($\mu g\ m^{-3}$)	MB ($\mu g\ m^{-3}$)	NME (%)	NMB (%)	RMSE ($\mu g\ m^{-3}$)
Winter	7	0.58	0.56	0.14	-0.02	23	-4	0.17
Spring	12	0.63	0.65	0.08	0.02	13	4	0.10
Summer	10	0.58	0.65	0.09	0.07	15	12	0.11
Autumn	3	0.58	0.65	0.10	0.07	17	11	0.10
Total	32	0.60	0.63	0.10	0.03	16	5	0.12
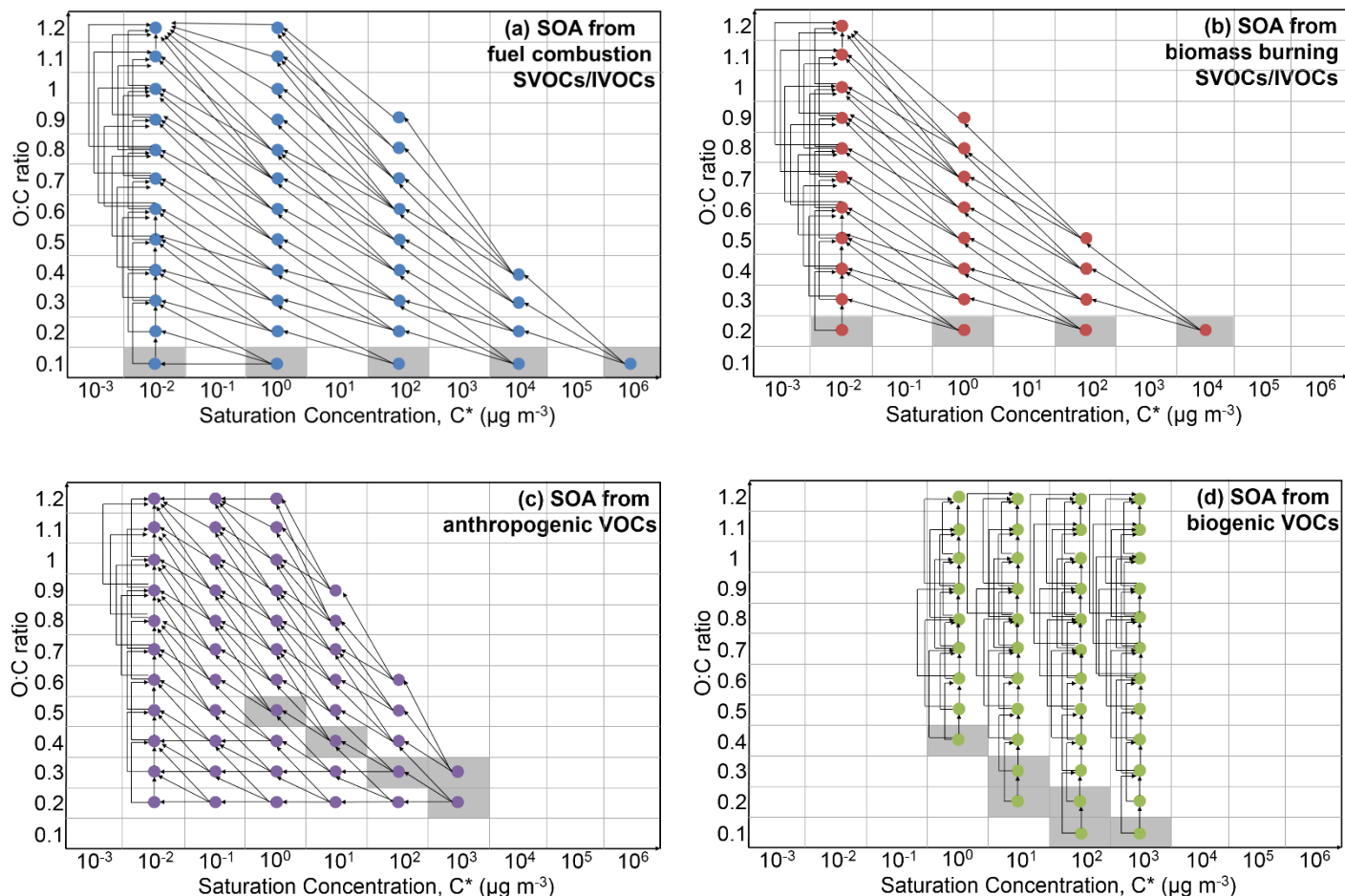
Figure 1: The 2-D grid space in ORACLE 2-D module with saturation concentration (in μg m^{-3}) on the x-axis and the O:C ratio on the y-axis. For each cell an organic surrogate compound is defined with a specific carbon number calculated as a function of effective saturation concentration and O:C ratio. The formation and evolution of SOA from: **(a)** fuel combustion SVOCs and IVOCs, **(b)** biomass burning SVOCs and IVOCs, **(c)** anthropogenic VOCs and, **(d)** biogenic VOCs are shown. The arrows correspond to the aging reactions and the grey grids to the initial chemical state of the species prior to aging.
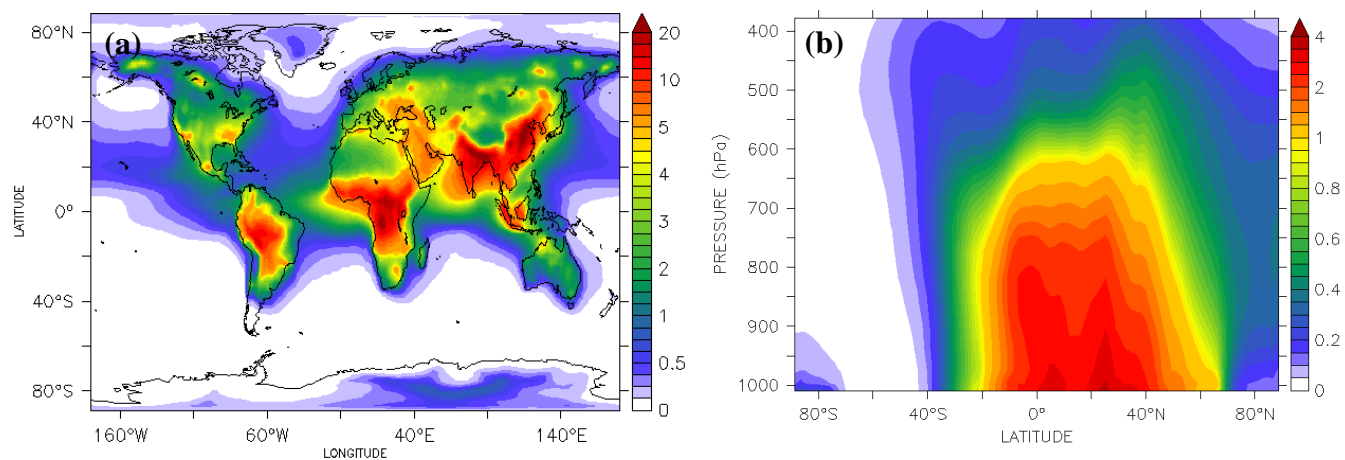
1032   **Figure 2:** Predicted average **(a)** surface and **(b)** zonal concentrations of total OA (in μg m^{-3})

1033   during the years 2001-2010.

1034

1035

1036

1037

1038
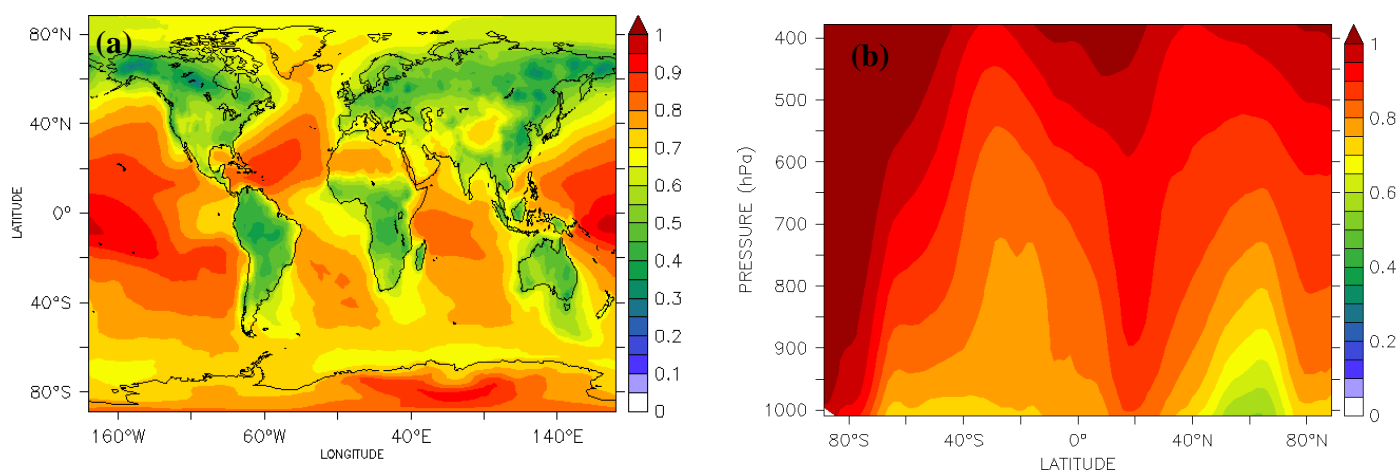
1039

1040 **Figure 3:** Predicted average **(a)** surface and **(b)** zonal O:C of total OA during the years 2001-
1041 2010.
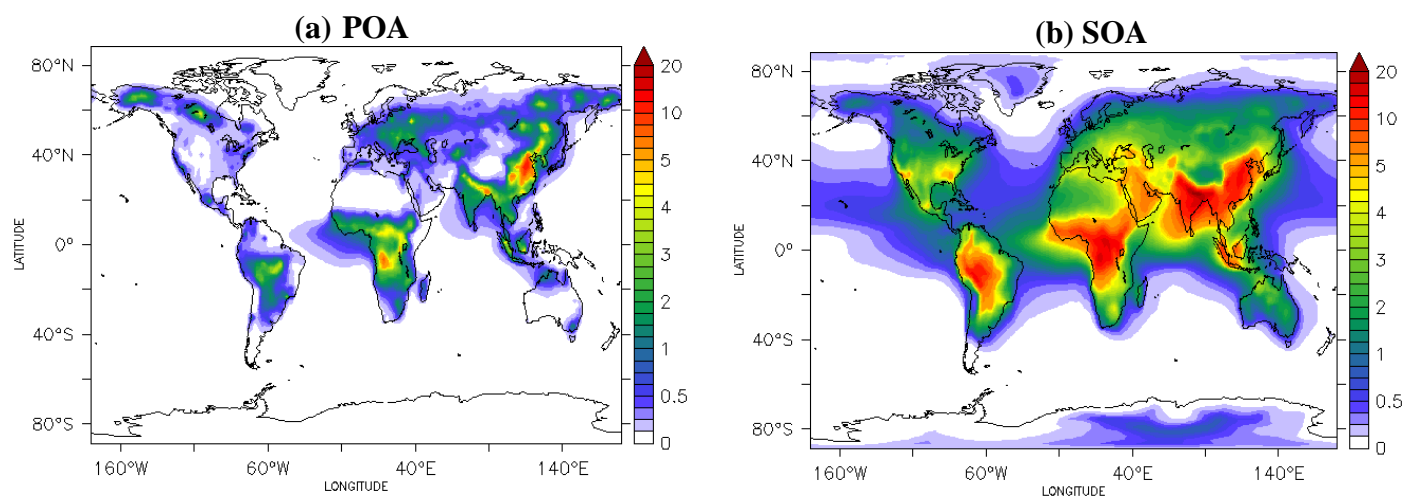
1042 **Figure 4:** Predicted average surface concentration (in μg m^{-3}) of **(a)** POA and **(b)** SOA during

1043 the years 2001-2010.
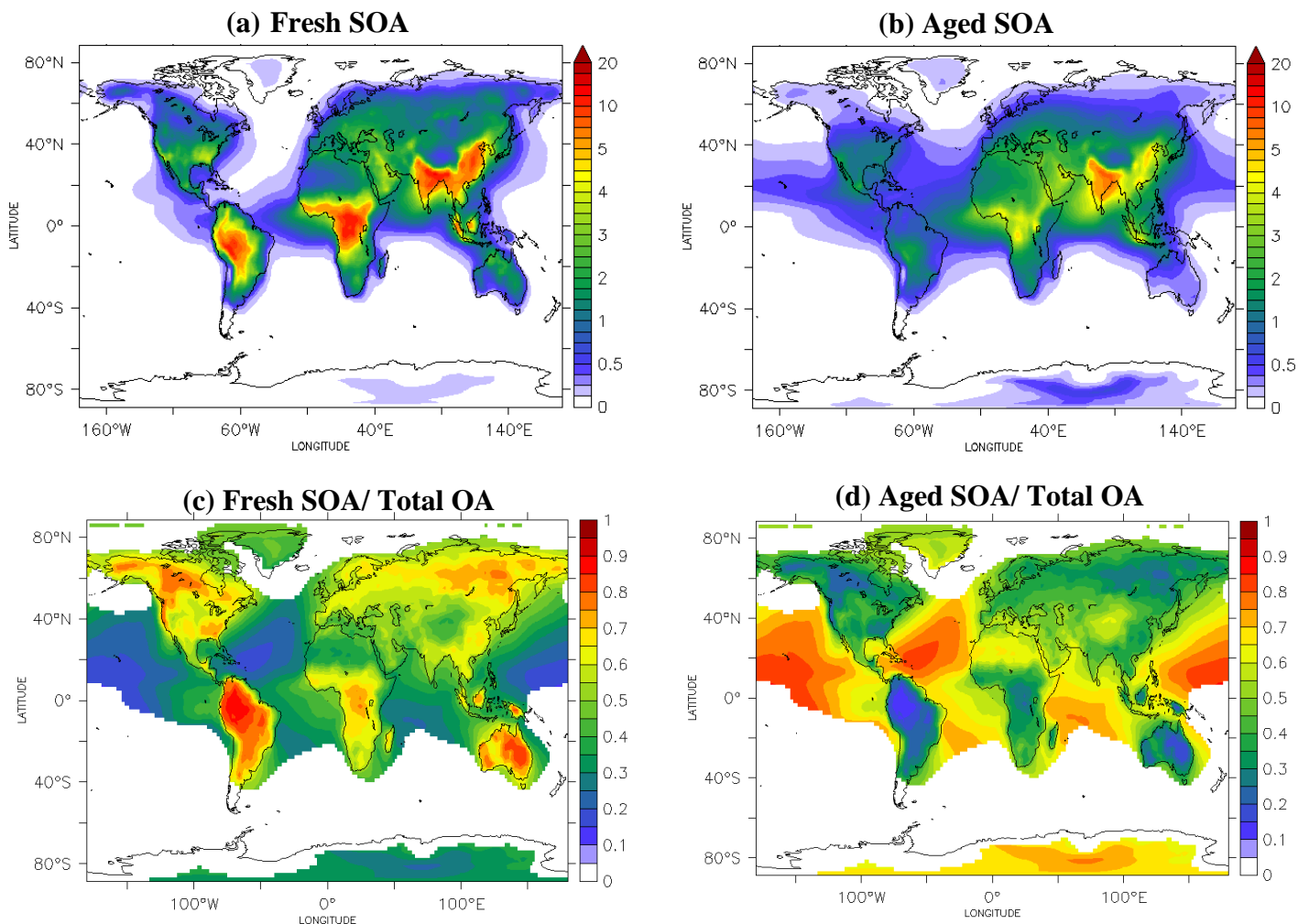
1044

Figure 5: Predicted average surface concentration (in μg m^{-3}) of **(a)** fresh SOA and **(b)** aged SOA and surface fraction of **(c)** fresh SOA and **(d)** aged SOA to total OA during the years 2001-2010.
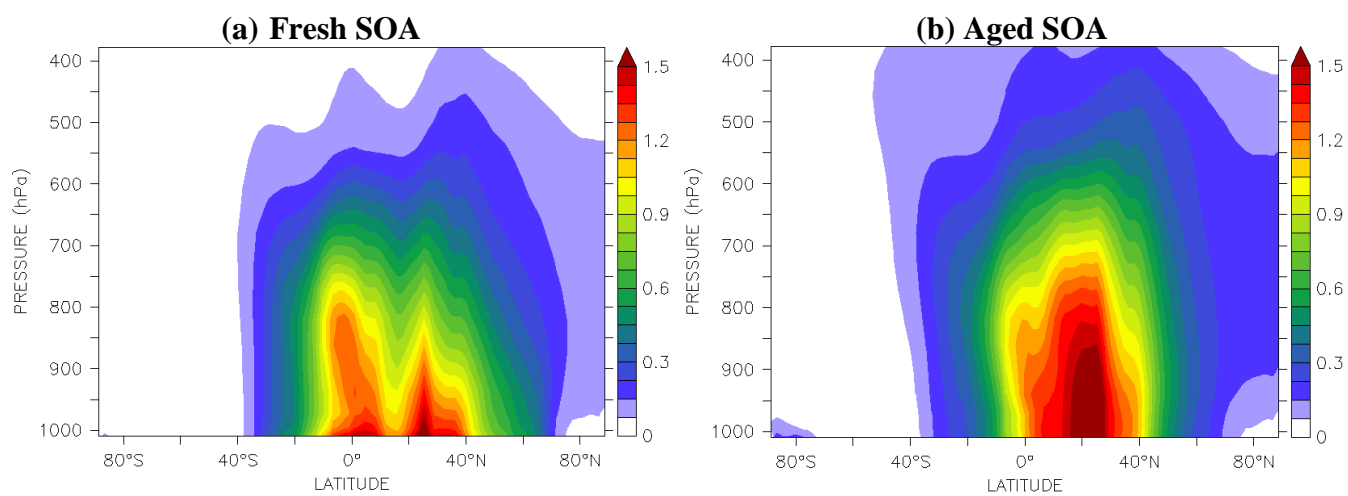
1048   **Figure 6:** Predicted average zonal concentration (in μg m^{-3}) of **(a)** fresh SOA and **(b)** aged SOA
1049   during the years 2001-2010.
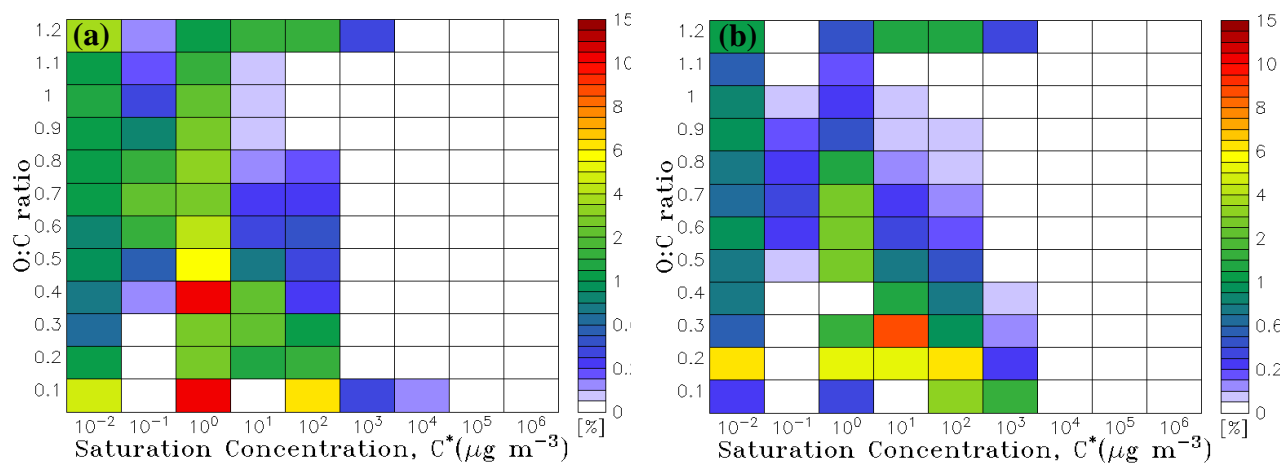
Figure 7: Predicted average fraction of OA concentration in each cell of the ORACLE 2-D grid space to total OA concentration over **(a)** Europe and **(b)** the Amazon basin during the years 2001-2010.

1053
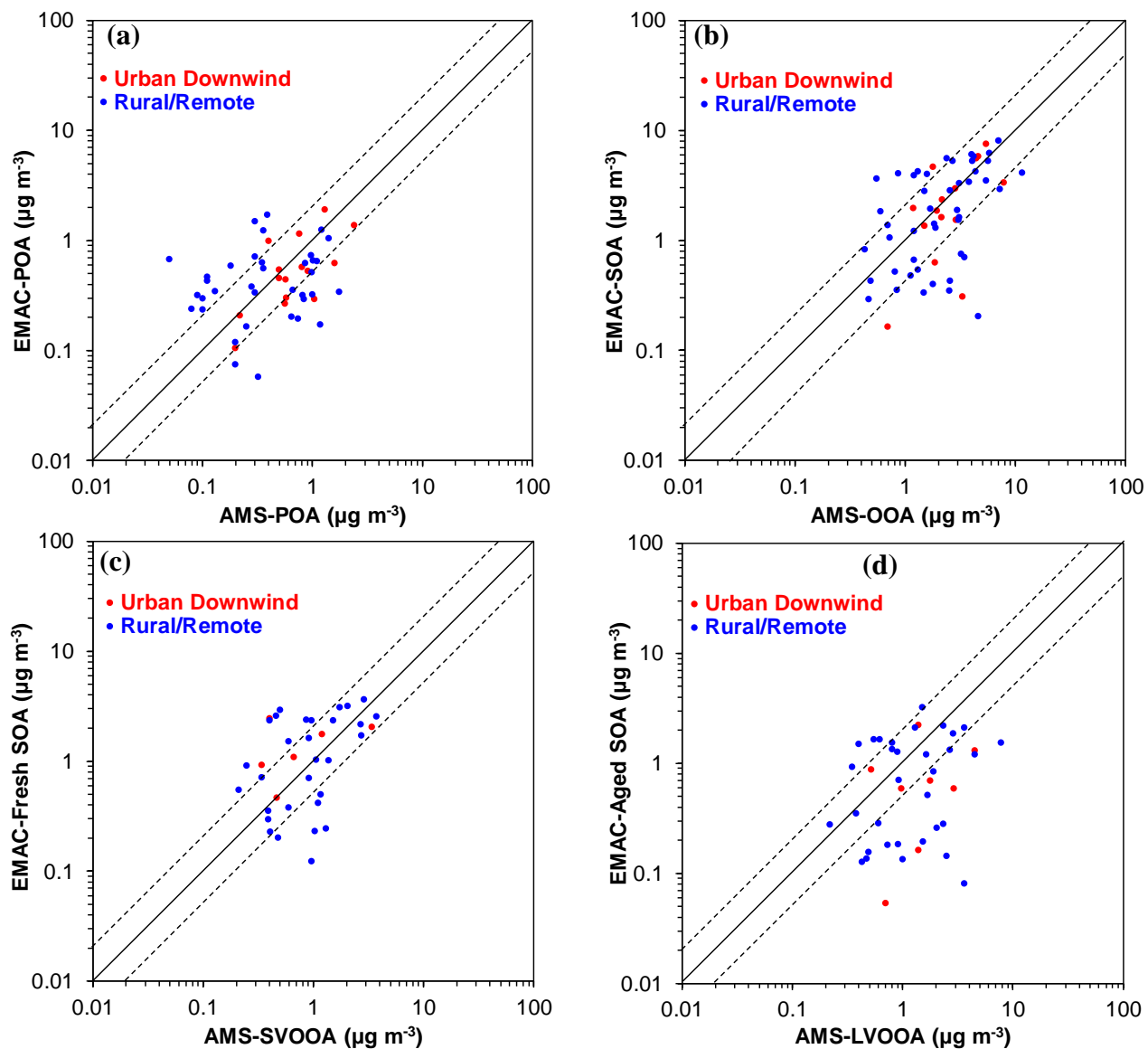
Figure 8: Scatterplots comparing model predictions to AMS measurements and their PMF analysis for: **(a)** POA, **(b)** OOA, **(c)** SVOOA, and **(d)** LVOOA concentrations (in μg m^{-3}) in the Northern Hemisphere during 2001-2010. Each point represents the data set average value over urban downwind (in red) and rural/remote (in blue) sites. Also shown are the 1:1, 2:1, and 1:2 lines.

1059
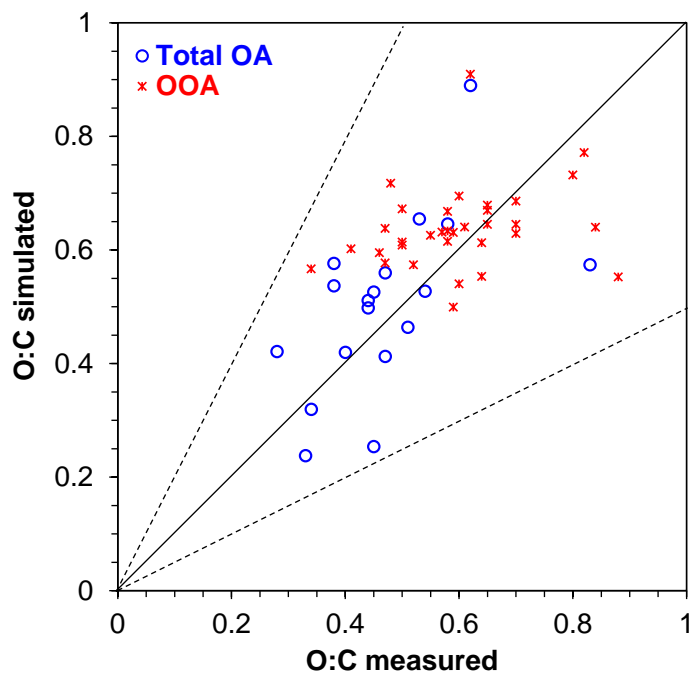
1060   **Figure 9:** Scatterplot comparing model predictions to measurements for O:C ratio of total OA
1061   (in blue) and OOA (in red) over non-urban areas in the Northern Hemisphere during 2001-2010.
1062   Each point represents the data set average value over a specific measurement site. Also shown
1063   are the 1:1, 2:1, and 1:2 lines.

1064

1065